

8-2010

Fiber optic chip for fully-guided Raman interrogation of molecular adsorbates.

Jennifer Burnett
University of Louisville

Follow this and additional works at: <https://ir.library.louisville.edu/etd>

Recommended Citation

Burnett, Jennifer, "Fiber optic chip for fully-guided Raman interrogation of molecular adsorbates." (2010). *Electronic Theses and Dissertations*. Paper 180.
<https://doi.org/10.18297/etd/180>

This Master's Thesis is brought to you for free and open access by ThinkIR: The University of Louisville's Institutional Repository. It has been accepted for inclusion in Electronic Theses and Dissertations by an authorized administrator of ThinkIR: The University of Louisville's Institutional Repository. This title appears here courtesy of the author, who has retained all other copyrights. For more information, please contact thinkir@louisville.edu.

**FIBER OPTIC CHIP FOR FULLY-GUIDED
RAMAN INTERROGATION OF
MOLECULAR ADSORBATES**

by

Jennifer Burnett

B.S., University of Kentucky, 2005

A Thesis Submitted to the Faculty of the

Department of Physics and Astronomy

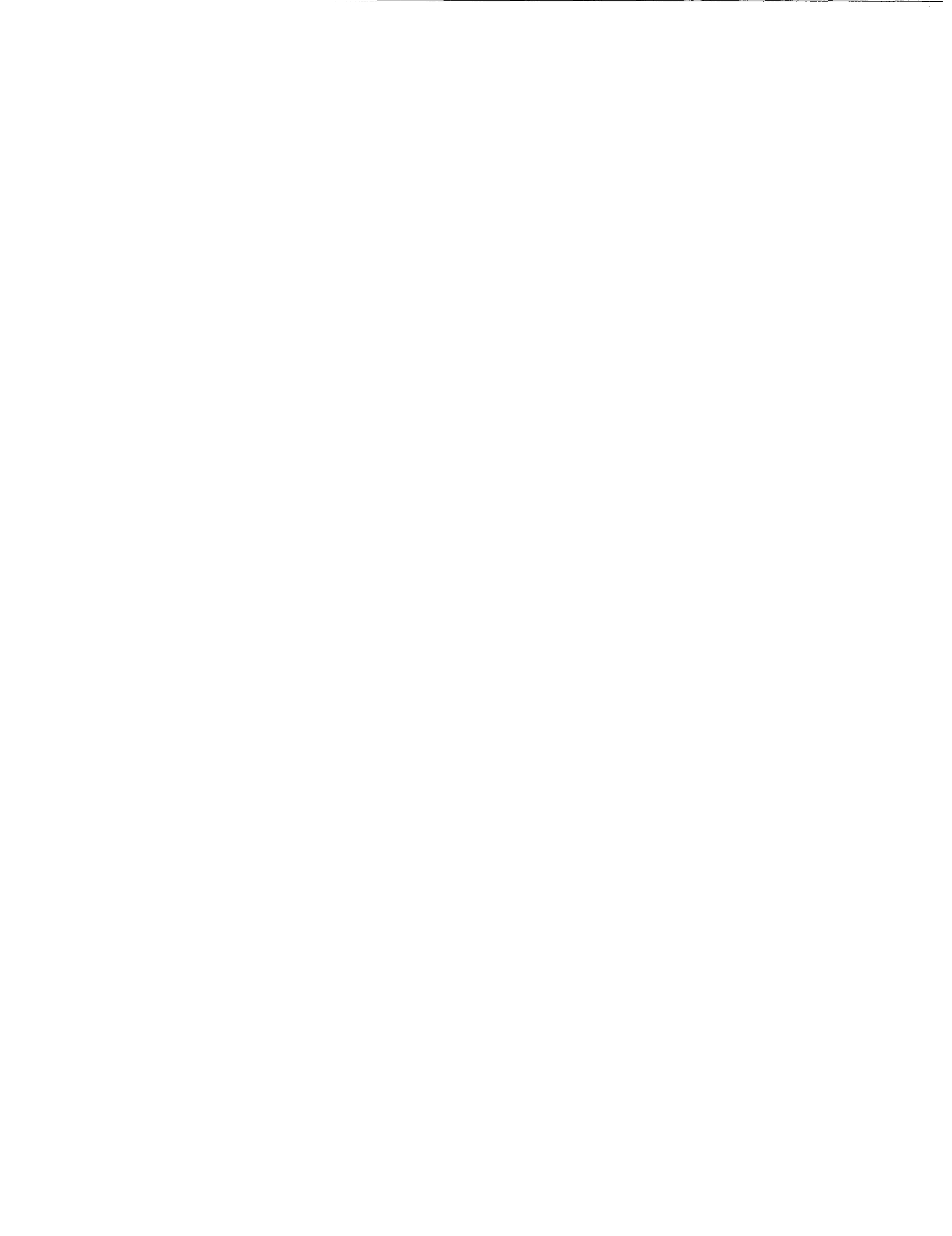
in the College of Arts and Sciences

of the University of Louisville

in Partial Fulfillment of the Requirements for the Degree of

Master of Science

August 2010



**FIBER OPTIC CHIP FOR FULLY-GUIDED
RAMAN INTERROGATION OF
MOLECULAR ADSORBATES**

by

Jennifer Burnett

B.S., University of Kentucky, 2005

A Thesis Approved on

August 3, 2010

by the Following Thesis Committee:

Dr. Sergio B. Mendes

Dr. Gamini U. Sumanasekera

Dr. Francis P. Zamborini

ACKNOWLEDGEMENTS

I would like to acknowledge with sincere appreciation the guidance and support I have received from Dr. Mendes both in academic pursuits and with research methods. Thank you for your patience and direction. It has truly been a terrific experience to work in this lab with such focused and clever individuals. Without the diligent work of both Nathan Webster and Joey Lynch I would not have any devices to study, so it goes without saying I appreciate all of your hard work.

Additionally, I would like to thank Dr. Sumanasekera and his group along with Dr. Jacek Jasinski for their collaborations and instruction. Thank you to Dr. Zamborini and Srinivas Beeram for the many hours of supervision and assistance graciously offered to establish protocols for the fabrication of gold nanoparticles for this project.

Finally thank you to my family and friends who have supported me without question. Your encouragement has been my motivating factor throughout every phase of my life.

Acknowledgement should be given to KSEF which has financially supported the bulk of this work.

ABSTRACT

FIBER OPTIC CHIP FOR FULLY-GUIDED RAMAN INTERROGATION OF MOLECULAR ADSORBATES

Jennifer Burnett

August 3, 2010

Planar fiber-optic chips (FOC) take advantage of the evanescent field effects of side-polished fibers, exhibiting usefulness in fluorescence, absorbance, electrochemical investigations, and as presented here Raman spectroscopy. The fabrication of the FOC utilizes a side-polishing process of a multi-mode optical fiber. The fiber core is exposed creating a D-shape when viewed laterally. The cylindrical fiber is mounted in a V-groove of a Si-wafer and side-polished, creating a platform for easier analyte handling with greater control over surface chemistry. A longer path length when compared with end-tip fiber probes results in a larger cross section of analyte signal. This work presents decoupled investigations of excitation and collection of Raman scattering using the FOC, for bulk media and thin films. Realization of a fully in-line system would alleviate the need for alignment of cumbersome bench-top optics, further increasing the utility of this device by allowing for interrogation of remote, hostile environments.

TABLE OF CONTENTS

Acknowledgements...	iii
Abstract...	iv
List of Figures...	vii
Chapter 1: Introduction...	1
1.1 Raman Spectroscopy...	1
1.1.1 Theory of Raman Spectroscopy...	1
1.1.2 Surface Enhanced Raman Spectroscopy...	3
1.1.2.1 Localized Surface Plasmon Resonance...	4
1.1.2.2 Metallic Nanoparticles for SERS...	4
1.2 Optical Waveguide Theory...	5
1.2.1 Total Internal Reflection...	5
1.2.2 Attenuated Total Reflection...	8
1.2.3 Near-field Coupling...	9
1.3 Fiber Optic Probes...	10
1.3.1 Modalities, Fabrication, and Applications...	10
1.3.2 Fiber Optic Raman Probes...	12
1.3.3 The Fiber Optic Chip Device...	16
Chapter 2: Experimental Methods and Materials...	19
2.1 Fabrication of the Fiber Optic Chip...	19
2.1.1 Overview...	19
2.1.2 Device Materials and Assembly...	19
2.1.3 V-groove Etching Procedure...	21
2.1.4 Lapping Process...	22
2.1.5 Characterization...	24
2.1.6 Cleaning and Maintenance...	25
2.2 Seed Mediated Gold Nanoparticle Growth Method...	26
2.2.1 Overview...	26
2.2.2 Cleaning of Substrate...	26
2.2.3 Functionalizing of Substrate...	26
2.2.4 Gold Seed Solution...	27
2.2.5 Growth Solution...	28
2.3 Fabrication of Carbon Coated Copper Nanoparticles...	29
2.3.1 Substrate...	29
2.3.2 Copper Deposition...	29
2.3.3 CVD growth process...	29
2.3.4 Carbon Coated Copper Nanoparticle Characterization...	30

2.4 Analyte Deposition...31	
2.4.1 Rhodamine 6-G...31	
2.4.2 P-Aminothiophenol...31	
2.4.3 Carbon Coated Copper Nanoparticles...32	
2.5 Methods of Characterization...32	
2.5.1 TEM...32	
2.5.2 SEM...32	
2.5.3 Raman Spectra...33	
2.6 Optical Setup...33	
2.6.1 Data Acquisition...33	
2.6.2 Absorbance Measurements...34	
2.6.3 De-coupled Measurements...35	
2.6.3.1 Overview...35	
2.6.3.2 Excitation Scheme...35	
2.6.3.3 Collection Scheme...36	
2.6.3.4 Fluorescence Measurements...37	
2.6.4 Fully Guided System...38	
2.6.4.1 Overview...38	
2.6.4.2 Inline Coupler...38	
2.6.4.3 Annular Mask Experiment...39	
2.6.4.4 Higher-indexed capping layer...40	
Chapter 3: Results and Discussion...41	
3.1 Preliminary Work...41	
3.2 Rhodamine-6G Experiments...42	
3.3 Surface Enhancement of FOC...45	
3.4 Fully-Guided Raman Detection...49	
3.4.1 Initial Experiment...49	
3.4.2 Modifications to Alleviate Fluorescence...51	
3.5 Carbon Coated Copper Nanoparticle Experiment...55	
Chapter 4: Conclusions and Outlook...58	
4.1 Conclusions...58	
4.2 Future Work...59	
References...62	
Curriculum Vitae...66	

LIST OF FIGURES

- Figure 1-1** Diagram of Raman Scattering Energy Shift...1
- Figure 1-2** Acceptance Angle of Optical Fiber...8
- Figure 1-3** Fiber Optic Probe Design Variations...14
- Figure 1-4** Fiber Optic Chip Design...16
- Figure 2-1** Lapping and Polishing Apparatus...23
- Figure 2-2** Seed Mediated Growth Process for Gold Nanoparticles...27
- Figure 2-3** SEM Image of Gold Nanoparticles...28
- Figure 2-4** Optical Set-up for Collection and Excitation Schemes...36
- Figure 2-5** Side View of Annular Mask...39
- Figure 3-1** Fluorescence of BSA from FOC...42
- Figure 3-2** Absorbance of R6G from FOC...43
- Figure 3-3** Data collected by FOC with Raman Optical Set-up for R6G...44
- Figure 3-4** Raman spectra of p-ATP...47
- Figure 3-5** Raman spectra of p-ATP using FOC...47
- Figure 3-6** Intensity vs. Power Graph for Raman Excitation...49
- Figure 3-7** Raman Spectra of Optical Gel Using FOC...55
- Figure 3-8** Carbon-Coated Copper Nanoparticle Images and Data...56
- Figure 4-1** Numerical Approximation of E-field Enhancement...60

CHAPTER 1: INTRODUCTION

1.1 Raman Spectroscopy

1.1.1 Theory of Raman Scattering

Raman spectroscopy is a well-established analytical technique which identifies chemical and physical properties through interactions with the phonon modes of a particular analyte. Phonons are the quantized normal modes of the vibrational states of a molecule or of a solid. Because this oscillatory motion is harmonic, there exists a specific frequency of each vibrational mode. The phonon is defined in terms of quantized energy, as energy is a function of this vibrational frequency.

Raman scattering is generated by a monochromatic light source, generally a laser. Scattering occurs when the molecular system is perturbed by an impinging photon. When the photon is absorbed by a molecule in the ground vibrational state, Rayleigh scattering typically may occur, an elastic scattering event in which the photon is reemitted at the same energy. If, however, the photon promotes the molecule to an excited vibrational state, energy will be transferred to the molecule into a higher vibrational state and the reemitted photon will have less energy, equivalent to the quantized energy of one phonon. This phenomenon is referred to as Stokes scattering. Anti-Stokes scattering refers to a molecule already in an excited vibrational state. The absorbed photon gains the energy of one phonon and is reemitted as the molecule relaxes to the ground vibrational state. Anti-Stokes occurs with less frequency at room temperature since considerably

fewer molecules tend to exist in an excited state under ambient conditions.

Another approach is to consider the components of the molecule as being the electron cloud and the nuclei. As a light wave approaches the molecule, it appears as an oscillating dipole. The electron cloud is distorted on a time-scale which inhibits the more massive nuclei to equalize, creating a virtual excited state. This virtual excited state is unstable and the light is quickly scattered without any energy change. This is referred to as Rayleigh scattering. In a much rarer event, this virtual state invokes movement of the nuclei, altering the vibrational state of the molecule. If the molecule has been modulated from the ground state to an excited state, Stokes scattering occurs. Likewise if through the intermediate step of a virtual state the molecule relaxes to the ground state from an initial excited vibrational mode, then Anti-Stokes scattering will occur, as illustrated in Figure 1-1. The scattered light is emitted with an energy change, resulting in Raman scattering. Typically, only one in every 10^6 - 10^8 photons is Raman scattered. However, this does not negate the importance of Raman scattering [3].

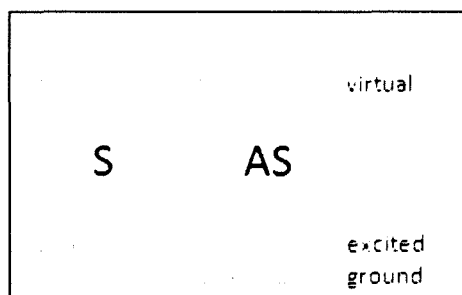


Figure 1-1 The upward arrows represent the energy of the incident laser light and the downward arrows represent the Raman scattering for Stokes (S) and anti-Stokes (AS).

Molecules may have up to $3n-6$ modes of vibration, where n is the number of atoms per molecule. Although the number of modes may reduce due to symmetry for certain molecular structures, this still gives many possibilities to variations in the

vibrational states. Raman spectra act as a molecular signature and can be quite complex considering the number of vibrational modes. These spectra offer much information as to the species of the molecule. Raman spectroscopy has been used to discern components in bulk sample, such as methanol in biogasoline [4], to detect the presence of bacteria [5] and for imaging of analytes tagged with Raman-active dyes [6].

Overlapping and interference between signals of multiple components in a complex sample is a major limitation for many spectroscopic methodologies. The FWHM of the spectral peaks of Raman-scattered emissions are quite narrow, creating a very discernable signature for the phase and species of an analyte. This allows for the valuable attribute of Raman spectroscopy to multiplex detection of complex samples. What is more is that Raman scattering can occur for any incident wavelength of light and the energy shift between the impinging and scattered light will remain consistent. This means data acquired with a He-Ne laser at 633-nm wavelength is comparable with scattering of a 405-nm wavelength laser line from a diode laser. The convention then is to plot Raman scattering on a wavenumber, ϖ , scale as energy is a function of wavenumber as represented in Equation (1):

$$(1) \quad \Delta E = h\Delta\nu = hc \Delta\left(\frac{1}{\lambda}\right) = hc (\varpi)$$

1.1.2 Surface Enhanced Raman Spectroscopy

As stated in the last Section, Raman scattering is very rare and as such competition with Rayleigh scattering and other optical signal such as fluorescence may cause difficulty in the detection of Raman scattering. Although filters may be inserted in the beam line to reduce the unwanted signal, a methodology to enhance the Raman signal

has been developed by use of localized surface plasmons produced by roughened metallic surfaces.

1.1.2.1 Localized Surface Plasmon Resonance

The effect of surface enhanced Raman spectroscopy (SERS) was first observed when the Raman spectrum of pyridine adsorbed to a roughened silver electrode was amplified. However, the mechanism behind the enhancement was not recognized at the time and still remains not fully understood today. The theory accepted currently involves amplification of the electric field in the area surrounding metallic nano-structures. When a metallic nanoparticle (NP) is irradiated by light, the E-field of the light causes electron cloud displacement. Coulomb restoring forces then induce an oscillation with a particular frequency associated with it. The E-field enhancement is related to the dielectric constant of the metal particle which is frequency dependent. Similar to a lightning rod, these structures induce a E-field enhancing corona effect that decays by the inverse of the cubed distance from the NP when treated as sphere with radius much less than the exciting wavelength [7].

Raman-active analytes in the presence of the amplified E-field will generate more Raman scattering. In turn, the scattered light may be amplified by the enhanced E-field. This two-fold effect of amplification of both the exciting wavelength and the emitted light leads to reported Raman signal enhancements of 10^6 [8], 10^{11} [9], and even 10^{14} resulting in single molecule detection [10].

1.1.2.2 Metallic Nanoparticles for Surface Enhanced Raman Spectroscopy

Analytical approximations have been useful in estimating the amount of enhancement as function of size, shape, and type of the metallic NP used. For spheroid

NP, with very small radii, r_{NP} , compared with the wavelength of light, λ , the problem may be treated electrostatically. The E-field, E_r , just outside the NP is then simply the solution to Laplace's equation and is a factor of the dielectric constants of the NP, ϵ_1 , and the medium surrounding it, ϵ_0 , the distance from the NP in Cartesian coordinates, and the frequency of the incident light, ν (see Equation 2) [3]. This solution only considers spherical NP, whereas numerical methods such as the discrete dipole approximation [11] rely on the polarizability of individual points within a lattice representing a NP of any shape. These methods however treat only single particles and aggregation is not considered, however they provide for a solid theoretical model of the SERS effect and provide some insight for substrate optimization [12].

$$(2) \quad E_r = E_0 \cos \theta \left[1 + \left(\frac{\epsilon_1 \nu - \epsilon_0}{\epsilon_1 \nu + 2\epsilon_0} \right) \left(\frac{r_{NP}^3}{r^3} \right) \right]$$

1.2 Optical Waveguide Theory

Synonymous to tubing that carries air, or channels that direct water, optical waveguides act as an infrastructure for electromagnetic waves in the optical region of the electromagnetic spectrum. Such mechanisms play an important role in directing a beam of light in a preferred direction. Of even more significance for this paper is the interaction of the light with material adsorbed to the boundary of the optical waveguide. Monitoring the changes in the light can offer information about the adsorbed analyte. It is important to review the fundamental theories behind these mechanisms to take full advantage of their nature for spectroscopic means.

1.2.1 Total Internal Reflection

Consider a light wave that travels through a uniform medium of refractive index, n_1 . The wave approaches a boundary of another uniform medium with an index of

refraction of n_2 . The incident wave may either reflect from the boundary or transmit into the second medium, or some combination of the two. Reflectance (R) is the portion of the incident light that is reflected. As shown in Equations (3) and (4), R is measured in terms of intensity as a square of the normalized electromagnetic amplitudes. Recalling that each wave is made up of an electric and a magnetic component, two polarization scenarios are considered. Any general case is a linear combination of the two possibilities of transverse magnetic (TM), when the magnetic field is perpendicular to the plane of incidence, and transverse electric (TE), when the electric field is perpendicular to the plane of incidence. Equations (3) and (4) give the reflectance for each case, where n represents n_2/n_1 , and θ is the angle of incidence.

$$(3) \quad R_{TE} = \left| \frac{\cos\theta - \sqrt{(n^2 - \sin^2\theta)}}{\cos\theta + \sqrt{(n^2 - \sin^2\theta)}} \right|^2$$

$$(4) \quad R_{TM} = \left| \frac{-n^2\cos\theta - \sqrt{(n^2 - \sin^2\theta)}}{n^2\cos\theta - \sqrt{(n^2 - \sin^2\theta)}} \right|^2$$

When considering the above equations, note that when $\sin^2\theta > n^2$ the argument of the radical becomes negative yielding an imaginary component to both equations. Taking into account the possible values of $\sin(\theta)$ range only from -1 to 1, this imaginary component may only occur when $n < 1$; in other words when the second medium has a lower index of refraction. The smallest such angle for which this is true is $\theta_c = \sin^{-1}(n)$, referred to as the critical angle, θ_c . When reflectance is calculated using an angle equal to or larger than the critical angle, one finds the value of R to be 1, meaning all of the light is reflected. This is true for both TM and TE polarized light. When the incident wave

approaches the boundary at the critical angle or larger, total internal reflection (TIR) occurs. This phenomenon sets the foundation for optical waveguides as now it is possible to bounce the light back and forth between two boundaries when the appropriate angles and refractive indexes are used.

One important consequence of TIR is the creation of an evanescent wave that penetrates the n_2 medium, decaying at an exponential rate. This decaying E-field is dependent on the index of refraction of the two media, the wavelength of the incident light, λ , and the angle at which the wave strikes the boundary, θ . Equation (5) describes the E-field as it penetrates in the medium from the initial value at the boundary, E_0 [13]. No energy is transmitted by the evanescent wave to the n_2 medium, maintaining the fully reflected wave.

$$(5) \quad E = E_0 \exp\left\{-\frac{2\pi}{\lambda_1} \sqrt{(\sin^2 \theta - n_{21}^2)} Z\right\} \quad \text{where } \lambda_1 = \frac{\lambda}{n_1}$$

Fiber optic waveguides make great use of TIR as the mechanism by which the light is propagated through the fiber. The basic composition of an optical fiber is a cylinder of a homogenous medium of a given index of refraction, n_1 , that is surrounded by a second medium with a slightly lower refractive index, n_2 . These two media are called the core and cladding respectively. Consider a fiber that has been cleaved perpendicular to the longitudinal axis of the cylinder. Light may be coupled into the end of the fiber core. That light will propagate through the fiber core only when the angle at the core/cladding boundary is equal to or greater than the critical angle. For all other angles, the light will be refracted into the cladding. This creates a condition known as the cone of acceptance. The acceptance angle, φ , is measured from the normal of the fiber end and is the maximum angle at which light may enter and propagate through the fiber

core as seen in Figure 1-2. The cone represents the acceptance angle traced through 3-dimensions. The acceptance angle, ϕ , is a function of the numerical aperture (NA) of the fiber (see Equation 6), which itself is a function of the index of refractions of the core and cladding. This concept will come up again when discussing fiber optic probes in Section 1.3.

$$(6) \quad \phi = \sin^{-1}(NA) = \sin^{-1}\left(\sqrt{n_1^2 - n_2^2}\right)$$

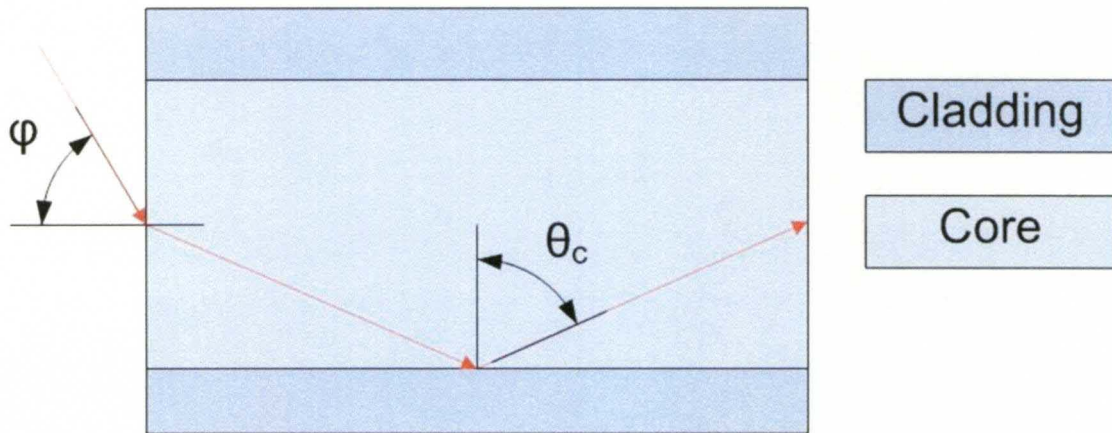


Figure 1-2 The acceptance angle is a function of the numerical aperture of and determines the amount of light to be coupled into an optical fiber.

1.2.2 Attenuated Total Reflection

The evanescent field created by TIR may be used to investigate analyte interactions at a boundary in a method referred to as attenuated total reflection. When an analyte is placed at the boundary between the n_1 and n_2 media, some of the light may be absorbed by the analyte resulting in an attenuation of the light that was initially totally reflected. The well established technique of ATR lends properly to the fiber optic

structure. Take for example a fiber that has had the cladding removed and an analyte adsorbed to the surface of the core. TIR is maintained if the core is surrounded by a dielectric medium with a smaller index of refraction such as air or water. Through the mechanism of ATR, at every point where the excitation light reflects from the boundary, an evanescent wave penetrates the analyte and the reflected light intensity is attenuated. The more reflections the more chances for an evanescent wave to interact with an analyte. This interaction may be recognized as a measure of absorbance.

As the intensity of the electric field exponentially decays with respect to the z -axis, a value referred to as the penetration depth may be defined. Penetration depth, d , is defined as the distance into medium at which E is a specific percentage of E_0 . This value is important when considering how much of the analyte interacts with the exciting light. Penetration depth ultimately depends on the nature of the analyte species, bulk or thin film. For thin-film cases, the evanescent field may extend beyond medium 2 into a third medium, say water or air. The index of refraction of third medium will also factor into the value of E and thus the value of d .

1.2.3 Near-Field Coupling

Consider again the scenario of an optical fiber which has had the cladding removed, yet TIR is maintained by a second medium of lower refractive index. If a molecule is adsorbed to the surface of the optical fiber core, as described above, ATR can occur through optical absorption by the analyte molecules. In addition to this effect, the molecule may also emit light as a result of returning to the ground state. In this case, it would be advantageous to capture the emission for spectroscopic studies. However, in principle, Snell's law inhibits the scattered light of the molecule from being guided by the

optical fiber as the refracted angle will never reach the critical angle.

This hindrance is surpassed by the mechanism of near-field coupling. If the adsorbate emits an evanescent field that overlaps with the evanescent field created by TIR of the fiber, then the molecule's emitted radiation may be coupled to the guided modes of the optical fiber. The largest limitation on this phenomenon is the distance from the center of the fiber core. The analyte must be close enough to the fiber to feel the effects of the evanescent excitation wave. Likewise, it must be close enough that a sufficient amount of its evanescent emission overlaps with the excitation field. This mechanism sets the foundation for a fully-guided spectroscopic device which uses a single optical fiber to both excite and collect optical emissions from an analyte.

1.3 Fiber Optic Probes

1.3.1 Modalities, Fabrication, and Applications

Fiber optic probes are well-established analytical tools and have been particularly useful in chemical sensing applications, specifically as a means of water detection [14], monitoring temperature fluctuations [15], sensing pH levels [16], and to measure Penicillin levels through enzyme-catalyzed reactions [17]. Fiber optic probes have also been demonstrated as valuable for the detection of toxins in the food supply industry [18], as a sensing mechanism of pesticides [19], and for use in biomedical applications [20-21] as they are preferential to the enzyme linked immunosorbent assay (ELISA) method with respect to time. Using commercial detection equipment, these applications can easily be adapted to become portable.

The use of fiber optics has many advantages in the field of spectroscopy. Generally, systems utilizing fiber optic probes offer ease of use with little need for

external utilities such as high voltage power supplies or pneumatic, vacuum, or coolant systems. When compared to an electrical system, there is less worry of interfering signals such as RF which can cause electrical equipment to short or malfunction. Certainly the ability to carry light and thus information over some distance with little loss is a beneficial attribute. This feature also allows for sensing in hostile and remote environments.

One real advantage of fiber optic probes is the ability to create a fully-integrated system that both excites and collects signal from an analyte. There are two major mechanisms by which fiber optic probes generate and collect optical information. The first mechanism is to deliver light to a sample by an optical fiber and collect the backscattered signal. Typically fabrication for such probes is simply to cut and polish the fiber transverse plane, known as the fiber tip. Fiber probes fabricated in this way are referred to as end-tip probes. The distal end is then submerged into a bulk medium or held a short distance away from the analyte and an exciting light source is delivered to the sample by the fiber. The emitted light from the sample is captured either by the same optical fiber or a separate fiber specifically for signal collection. Though these endoscopic devices offer the benefit of transmitting data to and from remote areas, they collect only the emitted signal which enters the cone of acceptance of the optical fiber, limiting the sensitivity of the device.

The second mechanism by which optical fiber probes generate and collect the signal from an analyte is through the processes of ATR and near-field coupling. Fabrication of these probes involves removal of the cladding of the fiber to expose the core. One method of fabrication for such probes is by tapering the tips of the optical fiber.

Tapered tip probes involve a gradual taper in the cladding diameter until the exposed core is reached [19]. Although collection of emitted backscattered signal is still possible through the distal end of such probes, the exposed core of the tapered surface now offers the potential for interactions with an analyte adsorbed to the surface of the fiber tip. Other fiber configurations remove the cladding along the longitudinal axis of the fiber. Either the cladding is completely removed to create a cylinder of only the core in the middle [22], or cladding is removed asymmetrically creating a D-shape if viewed from the side. [23-24]. For the fiber with the cladding removed completely, a heating and stretching method may be used to taper the core creating a bow-tie shape [25]. Like the tapered end tip probes, these longitudinally exposed fiber geometries make it possible for interactions with an immobilized analyte at the core boundary to occur. However, the longitudinal based fibers have an additional advantage in that they have a larger active area creating a higher cross section for detection.

Exposure of the core of the fiber allows analytes adsorbed to the surface of the fiber probe to interact with the evanescent field of the excitation light. ATR may occur and absorbance measurements can be obtained. Additionally, the evanescent field may induce spectral emission from the analyte such as fluorescence or Raman scattering. Through near-field coupling the emitted signal may be coupled back into the fiber and sent to a detection mechanism.

1.3.2 Fiber Optic Raman Probes

For the work described in this paper, the application of fiber optic probes for Raman spectroscopy is of the greatest interest. Section 1.1 highlighted the benefits of Raman scattering as a multiplexed detection mechanism. The utility of Raman

spectroscopy is ever increasing when coupled with the benefits of optical fiber probes as just described above.

As described in Section 1.3.1, fiber end-tip optic probes rely on a back-scattering signal from the analyte to be captured by a set of collection fibers. End-tip fiber probes have been used for some time in the excitation and collection of Raman scattering. Mimicking the configuration of a conventional Raman machine, the fiber probe delivers the excitation light to the sample and the scattered signal of the analyte is then collected by a set of surrounding fiber optics bundled to the initial probe fiber or is collected into the same fiber; the excitation signal is typically filtered out at the detection end by a notch filter [26]. These probes have been developed for hydrocarbon detection and quantification in aqueous solutions as well as in gasoline [27], for in vivo bio-sensing applications [28], and for the mapping of metastases in brain tissue [29]. Also, a Raman scattering based probe has been developed to monitor liquid nitrogen purity for the space industry [30]. Operating in a cryogenic media is evidence to the harsh environments in which these sensors can operate.

This methodology does not make use of evanescent field effects, and does little to diminish the requirements of precise optical alignment. One approach to this problem has been to add a ball lens to the tip of the fiber probe effectively increasing the amount of signal collected [31]. This set-up essentially creates an endoscopic technique that touts portability and usefulness for in situ biomedical investigations. However, the primary limitation to the end-tip probes is the acceptance angle of optical fiber allowing only a portion of the emitted signal to be collected.

For fiber probes which make use of a secondary optical fiber or bundle of fibers

for the signal collection, the acceptance angle of the excitation and collection fibers do not readily match lowering the cross-section for analyte detection. The analyte directly beneath the excitation fiber will emit the most signal, only a portion of which will reach the cone of acceptance of the collection fiber. To counteract this issue, a method has been developed to bevel the tip of the fiber allowing for a partially deflected output beam effectively changing the reach of the excitation beam and thus the resultant emitted signal of the analyte [1]. This beveled modification is pictured in Figure 1-3. In ambient air, such beveled-tip probes have been shown to double signal intensity when compared with the flat end-tip geometry [32].

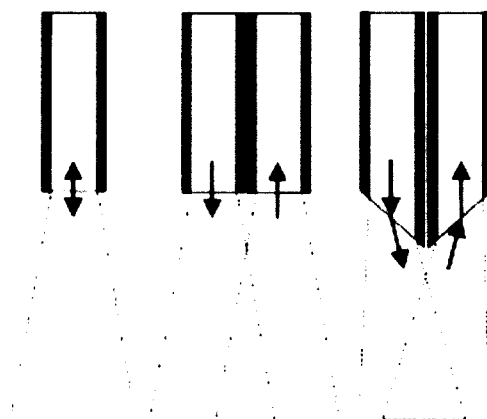


Figure 1-3 From left to right, end-tip fiber probe, end-tip fiber probe with separate excitation and collection fibers, and beveled end-tip probe [1].

Although these modifications have provided for improved signal intensity, fiber optic probes with an exposed core over a section of the fiber offer the advantage of alleviating optical alignment all together by making use of mechanisms such as ATR and near-field coupling. Additionally, the surface of such probes may be functionalized for

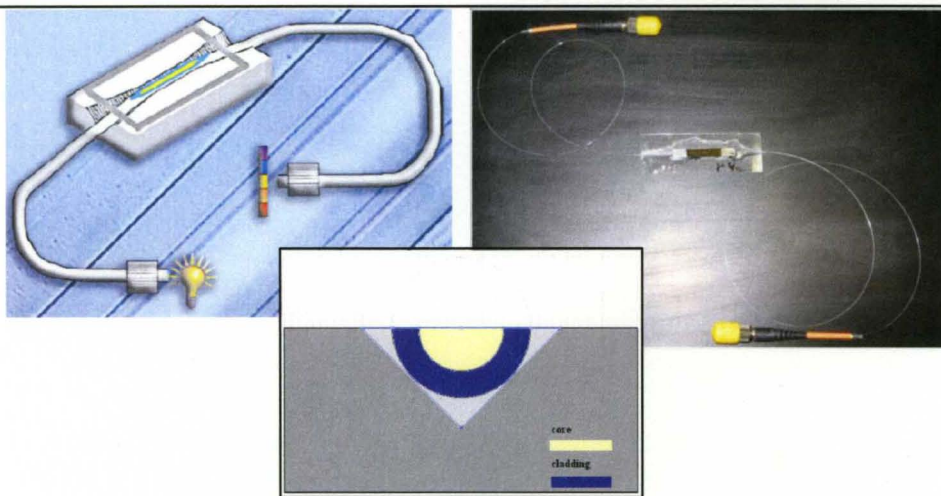
surface enhancement.

Stokes and Vo-Dinh have developed an exposed core fiber optic probe functionalized with silver for SERS investigations [33] that relies on evanescent field interactions with immobilized analytes. The fiber maintained the geometry of the end-tip fiber, but the cladding was removed from the end approximately 1 cm in length. A thin film of brilliant cresyl blue (BCB) was allowed to dry on the fiber tip, and the resultant Raman spectra of the thin film was compared with the signal of a BCB thin film collected by a conventional Raman machine. The signal-to-noise ratios were comparable between the two systems. Aqueous in situ Raman measurements were obtained using the same fiber, demonstrating the ability to probe bulk materials as well. This probe used a single fiber for excitation and collection to create a fully in-line system. The set-back in the design of this fiber probe is in the fragile exposed core of the end-tip. The geometry of a side-polished fiber optic probe would provide greater stability to the fiber probes as well as create a larger active area and thus a larger cross section for analyte interactions.

Recently, Zhang et. al. have demonstrated the use of a D-shaped fiber for excitation of Raman peaks of the dye Rhodamine-6G (R6G) [34]. The surface of the fiber was functionalized with a silver colloid mixture to produce surface enhancement, and the exciting light was guided through the fiber to generate R6G Raman spectra. The signal was collected by a conventional Raman machine. For comparison, the same substrate was then excited and collected by the conventional machine. The R6G spectra were compared and it was noted that the center peaks remained consistent regardless of excitation beam orientation, however this work was unable to demonstrate collection of the Raman signal by the fiber. A fully in-line system that makes use of the planar geometry of the side-

polished D-shape fiber would be the next logical step in the development of fiber optic Raman probes.

Figure 1-4 The FOC excited by a white light source (left); a transverse view of the D-shaped fiber (center); an aerial view of the FOC (right)



1.4 The Fiber Optic Chip Device

The work of this paper centers around a device termed the fiber optic chip, FOC. This apparatus is based on a D-shaped, side-polished fiber optic platform. The FOC is a modified version of the first generation device developed at the University of Arizona [35]. The FOC is fabricated by a polishing procedure which exposes the core of a multimode fiber as pictured in Figure 1-4. The exposed core region of the fiber is mounted in the etched groove of a Si-wafer. The wafer creates a platform useful for analyte deposition, lending well to thin film applications; in addition it provides a convenient geometry to developing an array of transduction probes. Through the mechanism of ATR, the FOC makes use of evanescent waves at the boundary of the core to optically excite the adsorbed species, and the emitted signal from an analyte is collected via near-field coupling. This fully guided device uses a single fiber to deliver the excitation beam and retrieve the scattered signal, eliminating the need for

cumbersome bench-top optics and more importantly their mechanical alignment, freeing the device to remote applications. Additionally, the D-shaped fiber provides a larger active area when compared to tapered tip fiber optic probes, translating into a greater probability that an analyte will interact with the evanescent field of the exciting light. Demonstrations of absorbance measurements and the monitoring of electrochemical properties have been made using the FOC [35-36]. Additionally, the FOC has been used to excite and collect fluorescence as detailed in Chapter 3.

The goal of this project is to extend the utility of the FOC to include Raman spectroscopy. The ability to use a single device to interrogate a sample according to multiple optical spectroscopic techniques is of great interest. As outlined in the previous Section, fiber optic end-tip probes have been employed for Raman investigations but do not make use of the ATR mechanism employed in a tapered tip or side-polished fiber. An additional motivation for a side-polished Raman platform is to make use of the flat geometry of the device for easier analyte handling. The planar geometry allows for control of the surface chemistry and creates a platform which may easily be functionalized with metallic nanoparticles for surface enhanced Raman scattering. Some work toward a D-shaped Raman platform has been forged, yet only excitation of the Raman signal has been demonstrated [34]. The prospects of this project set out to both excite and collect Raman scattering using the fully integrated system of the FOC.

In addition to demonstrating that the FOC may be used as a device for Raman spectroscopy, an application of graphene as an indirect mode of analytical sensing will be explored. Graphene is very thin, measuring as low as 1 Angstrom thick, and will work well within the range of the evanescent field at the surface of the exposed fiber. Graphene

has very strong Raman features that may shift in the presence of certain chemicals. Through changes in the local carrier concentration of graphene, gas-phase analytes such as nitrogen dioxide, carbon monoxide, ammonia, and water vapor have been detected at very low limits by resistance monitoring [37-38]. Raman shifts as a function of electron doping [39] gives promise to the use of graphene as a sensing agent. By functionalizing the surface of the FOC with graphene, variations in the graphene spectrum may be used to give information about adsorbates on the surface of the graphene.

CHAPTER 2: EXPERIMENTAL METHODS AND MATERIALS

2.1 Fabrication of the Fiber Optic Chip

2.1.1 Overview

The fabrication of the fiber optic chip (FOC) begins with a small section of an optical fiber which is stripped of its jacket, exposing the cladding. This section of the optical fiber is then mounted in an etched V-groove of a Si-wafer which acts as a platform for spectroscopic investigation as well as supports the fragile stripped fiber. Through a lapping process, the fiber core is exposed producing a D-shaped fiber and completing the assembly.

2.1.2 Device Materials and Assembly

The optical fiber used for the body of this work was a multimode, step-index optical fiber (Thorlabs AFS50/125Y), with 0.22NA. The diameter of the core of the fiber is 50 μm and that of the cladding is 125 μm . Each FOC device began with a 1-2 m section of fiber. At the center of this section, a segment of the fiber is stripped of its jacket by carefully scraping parallel to the length of the fiber with a razor blade. After the jacket is removed, the fiber is washed with isopropanol.

A V-groove was etched in a Si-wafer by the process detailed in Section 2.1.3. The Si-wafer is diced into segments with approximate dimensions of 40 mm by 5 mm. The etching runs lengthwise through the middle of each segment. By itself the diced Si-wafer section is fragile, so each piece is adhered using a two part epoxy (Epotek 301) to a glass

substrate that has also been diced to the same dimensions. This assembly is then attached to a 2-degree tapered mount using a plasticized bonding wax (Logitech OCON-199) and polished with a 10% by weight 14 μm (1700 grit) slurry (Lapmaster LAPS-0002-005-1700). All polishing and lapping procedures were performed using a bench-mounted open-face lapping machine (Lapmaster Model 12) as described in Section 2.1.3. Tapering the edges of the Si-wafer allows the exposed fiber to fit in the V-groove fully taut. The Si-wafer is polished until the tapered region reaches approximately 11 mm from each transverse edge of the wafer. It is important that the taper extend far enough inward such that the fiber is able to seat properly without too much strain at the threshold of the jacketed portion. After the tapering process of the Si-wafer, the V-groove no longer transverses the entire length of the wafer. The length of fiber with the jacket removed should extend 1.7 mm from the onset of the V-groove on both sides. In this way, the tapering determines how long the exposed portion of the fiber should be.

To further strengthen this platform, the Si-wafer/glass assembly is fastened to a microscope slide using the Epotek 301 epoxy. The jacket-stripped/exposed-cladding portion of the fiber is laid into the V-groove etching. A small portion of jacketed fiber rests on each transverse edge of the Si-wafer to prevent breakage. Care is taken to ensure that the fiber does not bow upwards as a smaller bending radius of the fiber translates to an increased evanescent field [22]. The fiber is secured in the V-groove using the Epotek 301 epoxy, and from this point the lapping procedure proceeds as detailed in Section 2.1.4.

At the completion of the lapping procedure, standard FC connectors (FIS) are spliced to either end of the FOC and the device is tested for insertion loss using a standard diode laser (Thorlabs LDC5000).

2.1.3 V-groove Etching Procedure

A chemical etching process was used to create a channel in the Si-wafer to place the fiber. Due to the crystalline structure of Si, the resultant channel has two sloping walls forming a V shape.

Creating the V-groove begins with a 500 μm Si-wafer with a minimum of a 1 μm oxidized layer. A layer of HMDS primer followed by a layer of photo-resist (Shipley 1813) is spin coated on the wafer and cured on a hot plate. A slotted mask is placed on top of the wafer using a mask aligner (Süss MicroTec). The slots are of the desired width for the eventual V-groove. The masked wafer is then exposed to UV light for 7 seconds. The wafer is then placed in developer (Microdeposit MF-319) leaving photo-resist in the areas that the mask covered and exposing the wafer surface in the slot formation. The wafer is then covered in buffered oxide etchant (BOE) to erode the oxide layer of the exposed wafer, etching the masked pattern into the oxide layer. The BOE will remove 100nm/min of the oxidized layer, so at minimum the wafer should remain in the BOE for a period of 10 min. The remaining photo-resist is then removed using a solvent rinse. At this point, the oxidized portion of the Si-wafer is intact everywhere aside from a series of lines created by the slots of the mask; these lines have no oxidized layer.

In the final step, the V-grooves are formed through chemical etching. The Si-wafer is submerged in 45% KOH, which is set on a magnetic stirrer and heated to 55° C. It should be noted that the etching rate of the KOH increases with temperature. The KOH

etches the Si at a much faster rate than the SiO₂, therefore creating grooves only in the areas without an oxidized layer. The angle between the sloping walls and the face of the substrate, 54.74°, is set by the Si crystalline structure. Etching will terminate once the (1,1,1) plane is reached; therefore the depth of the V-groove is pre-determined by the width of the Si lines. The resultant V-groove is approximately 240 μm wide and 170 μm deep.

The etching process takes 15-20 hours. Once the chemical etching of the V-grooves is complete, the Si-wafer is diced into approximately 40 mm by 5 mm long strips with a V-groove running longwise through the center of each.

2.1.4 Lapping Process

As reported in the literature, the core of an optical fiber may be exposed by a chemical etching process or by a precisely controlled flame [40]. In this work we use a lapping process by which the cladding is slowly polished away exposing the core [14, 41-42]. Lapping of the substrate involves polishing it against a roughened material with an abrasive lubricant, referred to as slurry. This process slowly erodes material from the substrate. The Lapmaster, model 12, as pictured in Figure 2-1 was used for all lapping processes. The polishing plate, the roughened material used in the Lapmaster assembly, is made of serrated cast iron topped with a polyurethane mat and serves as the base of the set-up. A yoke holds a conditioning ring in place on the polishing place. A spindle carrier is fastened to the top of the conditioning ring and together the two serve as the base console in which the FOC is to be placed. The FOC is attached to a working disc using a plasticized bonding wax (Lapmaster OCON 1-99). The working disc is mounted to a spindle and fed into the spindle carrier/conditioning ring assembly. The spindle carrier

was specially machined with brass sleeve bearings to hinder a parallax motion of the spindle within the carrier. If this wobble is not corrected for, the FOC will not be polished evenly, the outer edges eroding at a faster rate.



Figure 2-1 Image of Lapmaster Model 12: spindle carrier held in place by yoke (A), slurry dispenser (B), and polishing plate (C).

To begin lapping, the polishing plate is rotated at an approximate rate of 20 rpm as the FOC is held in place by the yoke. A coarse grit slurry, composed of 1% 1- μm alumina powder (MetMaster SF-RF-1P), is dispersed in 16 s increments on the polishing plate. For all of our purposes, the solvent used for the slurry was de-ionized water. Periodic monitoring of the FOC should occur after durations of a half an hour to an hour

of lapping. As lapping takes place the epoxy will wear down exposing the cladding. Eventually the cladding will erode, exposing the core. Monitoring of the FOC should occur more frequently, every 15 minutes, once the width of the exposed cladding nears 100 μm .

When the measured width of the exposed cladding is approximately 115 μm , the slurry is changed to a fine grit, composed of 1% 0.5- μm cerium oxide (Logitech OCON 260). Lapping continues until the center of the fiber is reached, measuring approximately 125 μm across the width of the exposed cladding. Once lapping is complete, FC connectors are attached to the optical fiber ends on both sides of the device.

2.1.5 Characterization

The following methods are used to determine dimensions of the FOC components and monitor the polishing process. In the etching of the V-grooves, the ultimate depth may be calculated when the width of each groove is known. Using a surface profiler (Veeco Dektak 8), the depth is periodically monitored to ensure that the groove is fully etched. This device works much like an Atomic Force Microscope (AFM), only with a precision on the order of microns.

In the lapping process, one can determine when the polishing depth begins to approach the center of the fiber, creating the D-shape, using simple geometry. The depth to which the fiber has been polished is determined by measuring the width of exposed fiber. The width of the fiber is monitored using a standard optical microscope (VWR Vista Vision) and periodically measuring from the boundary of the cladding and epoxy on either side of the fiber. Three measurements are taken across the length of the exposed

fiber to ensure that the fiber is polishing evenly. Periodic monitoring also allows for early detection of breakages in the fiber.

2.1.6 Cleaning and Maintenance

Once the fiber is fully polished and connectors are attached, the FOC is ready to be used for spectroscopic measurements. Often this requires drop casting a solution on the surface of the FOC or allowing an analyte to dry to the FOC. Removal of these analytes is performed with a solvent wash and preferably dried under a nitrogen-flow. The use of acids or such removal methods a piranha solution are strongly discouraged because under such conditions the fiber is prone to breakage and the epoxy does not stand up well.

Maintenance of the FOC outside of general cleaning includes the repair of breaks to the optical fiber between the FOC and the FC connectors. Breakages are able to be repaired using a fusion splicing machine (Ericsson FSU 995 FA). To splice a fiber, it first must have the jacket removed. Acetone is used to soften the jacket and a stripping tool (Micro Electronics Microstrip) portion is removed using a length of the jacket. The exposed fiber is then given a clean cut using a fiber cleaver (Fitel Model No. S323). The two ends of fiber to be fused together are inserted in the splicing machine. The splicer emits a large spark between the two fiber ends, melting the fibers together. It should be noted that the given length of fiber to be spliced must fit stably in the splicing machine. This is approximately measured as 4 inches.

2.2 Seed Mediated Gold Nanoparticle Growth Method

2.2.1 Overview

The method of fabrication for gold nanoparticles used in the FOC experiments relied on a seed-mediated growth mechanism. The initial gold seed is prepared via a citrate reduction reaction of a gold precursor (HAuCl_4). The gold seed is then submerged in growth solution for a selectively determined time to achieve the desired size of individual nanoparticles. Figure 2-2 shows the process in its entirety.

2.2.2 Cleaning of Substrate

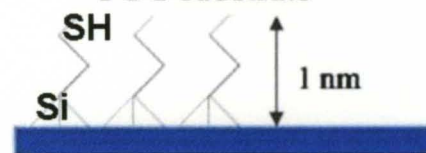
Prior to growing gold nanoparticles (AuNP) on the surface of the FOC, the substrate first needs to be free of any precipitates. As already mentioned, cleaning with a piranha mixture is not a viable option as the acids have a very quick corrosive reaction with the FOC materials, particularly the epoxy. Therefore, the FOC is cleaned using an ozone cleaner for 15 minutes to rid it of any organic materials.

2.2.3 Functionalizing of Substrate

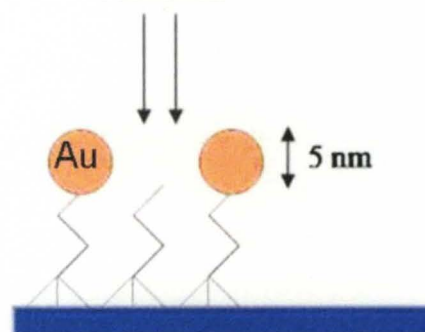
The surface of the FOC is functionalized using a solution of 10 mL of isopropyl alcohol (IPA), 3-4 drops of nanopure de-ionized water, and 100 μL of 3-mercaptopropyltrimethoxysilane (MPTMS). The substrate is submerged in the functionalizing solution, covered, and heated to just below 100°C on a hotplate. After 25 minutes the FOC is removed from the solution, rinsed with IPA, and dried under a nitrogen flow. It should be noted here that this step in the procedure proved to be quite damaging to the fiber. Later iterations of the procedure refrained from bringing the solvent to a boiling point, heating to 60°C (just below the glass transition temperature of the epoxy) while submerged in the solvent solution for a slightly longer duration.

MPTMS to functionalized

FOC substrate



Au Seed



Growth Solution

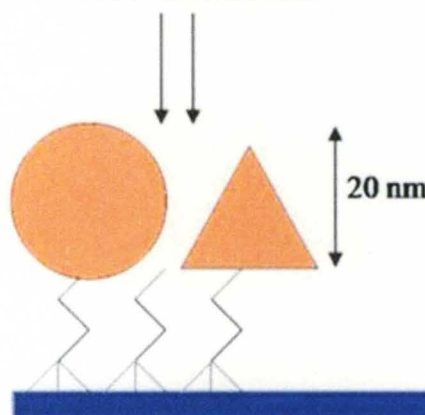


Figure 2-2 The seed mediated growth process as detailed in section 2.2. The gold seed is adsorbed to a functionalized substrate and then submerged in the growth solution for the creation of larger gold nanoparticles.

2.2.4 Gold Seed Solution

The gold seed solution is prepared by adding 0.5 mL of 0.01M citric acid, trisodium salt aqueous solution and 0.5 mL of 0.01M $\text{HAuCl}_4 \cdot 3\text{H}_2\text{O}$ to 19 mL of nanopure de-ionized water. Added to this is 0.6 mL of 0.1 M sodium borohydride that has been kept at 0°C . The color of the solution will turn reddish, indicating the nanoparticles

have been formed. The solution is mixed for 2 hours using a magnetic stirrer and will last approximately 5 hours. The FOC is then submerged in the seed solution. After 15 min, the FOC is removed from the seed solution, rinsed with nanopure de-ionized water, and dried under a nitrogen flow. The gold nanoparticles at this stage are on the order of 3-5 nm in diameter.



Figure 2-3 SEM image of gold nanoparticles created by the process described in section 2.2. Nano-scale spheroids, platelets, and rods are the by-product of the growth process. (Image provided by Srinivas Beeram.)

2.2.5 Growth Solution

Preparation of the growth solution: Separately, 9.00mL of 0.1M of Cetyl trimethylammonium bromide (CTAB) and 50 μ L of 0.1M ascorbic acid, both dissolved in water, are mixed via sonication. 450 μ L of the H₂AuCl₄ solution is added to the CTAB solution, resulting in a yellowish color change. The ascorbic acid solution is then added to the mixture, changing the color back to clear. The FOC is submerged in the growth solution for one hour. The FOC is then removed from the growth solution, rinsed with nanopure de-ionized water, and dried under a nitrogen flow. The transparent portion of the FOC should turn a purplish color, indicating Au nanoparticle growth. The resultant nanoparticles range in size and shape as shown in Figure 2-3.

2.3 Fabrication of Carbon-Coated Copper Nanoparticles

2.3.1 Substrate

The initial substrate chosen for this project was fused silica. For better graphene growth in the CVD process, a 5nm layer of alumina was deposited using a Cambridge Nanotech Savannah 100 ALD on some of the silica pieces. The rest of the nanoparticles were grown on a Si-wafer with a 300 nm oxidized top layer.

2.3.2 Copper Deposition

Copper is coated on the substrate by electron beam (e-beam) deposition using a KJL evaporator. In an evacuated chamber, the sample is secured to a platform that is then turned upside down, parallel with the ceiling of the chamber. An electron beam then bombards a Cu pellet creating a vapor of Cu. As the Cu is evaporated, the vapor rises, coating the sample mounted above. Varying thicknesses were deposited, 0.5, 1, 5, and 42 nm. It should be noted that the precision of the e-beam is on the order of 1 nm; therefore substrates with sub-nanometer thickness carry a large error associated with the Cu-layer thickness.

2.3.3 CVD growth process

A graphene layer is deposited on top of the Cu film using a chemical vapor deposition (CVD) growth process. CVD is a chemical growth technique in which a hydrocarbon gas flow is passed over a thin film metal substrate at high temperature, approximately 900 to 1000 °C. This method of carbon growth allows for large area carbon film growth, on the order of cm², to grow under ambient pressure conditions [43-44]. The resultant films range in thickness from monolayer to multilayer graphene.

The substrate is placed in a sample boat and pushed by a metal rod into the center

of a glass cylinder. The cylinder is then centered beneath the heat source in a tube furnace (Thermolyne 79300). A mixture of argon and hydrogen gas is streamed through the cylinder at a rate of 700 sccm to reduce oxygen on the surface of the substrate. The gas flow terminates in a beaker of water at the end of the cylinder. Monitoring bubbles in the water serves as a secondary flow check to ensure gas was being pumped through the chamber. The temperature of the furnace is increased at desired increments to a set point. The flow rate of the Ar/H mixture is then reduced to 160 sccm. Methane gas is then opened to the chamber at a rate of 20 sccm, initiating the growth process. After a set period of time, generally 4 minutes, the methane flow is cut off from the chamber while the Ar/H continues to flow at a low rate. The temperature setting of the furnace is reduced to room temperature, and the sample is removed once cooled.

The CVD process was varied by temperature ramp rate, growth time, and gas flow. Temperature ramping was generally set at a steady increase from room temperature to 950 °C, however a few experiments varied by first ramping to 300 °C and then to 950 °C. Additionally, the final set point was varied to 900 °C. Growth time, or the duration of the methane flow, varied from 2 to 10 minutes. Different purity levels of the H gas were used to rule out issues of contamination. Each parameter change was monitored in characterization to determine the optimal method of growth for our uses.

2.3.4 Carbon-Coated Copper Nanoparticle Characterization

The carbon-coated copper nanoparticles (CCuNP) were characterized by a variety of well-established techniques (see Section 2.5 for instrument details) to monitor physical changes as a function of variations in the growth procedure. Raman spectra of each sample were taken to determine if and in what form C growth had occurred. Raman

spectra helped discern between samples with monolayer graphene, multilayer graphene, amorphous carbon, and in some cases C nanotubes. Transmission electron microscopy (TEM) images were taken of each sample to further determine the nature of the C growth, and generally gauge the carbon to copper ratio for individual particles. Additionally the images were used to survey the consistency of the CCuNP in terms of diameter and shape, spherical, oblong, or faceted. The energy dispersive X-ray spectroscopy (EDAX) function of the TEM assembly was used to determine the sample composition to check for contaminants.

2.4 Analyte Deposition

2.4.1 Rhodamine 6-G

The Rhodamine 6-G (R6G) analyte was used only for absorbance measurements. R6G (95% purity, Sigma Aldrich) was analyzed in aqueous solution and as a dried film. Aqueous solutions of varying concentrations, 1 mM and 10 μ M, were drop cast onto the FOC along the exposed core. Care was taken to not pipe too much of the solution as its hydrophobic nature would cause it to run off. The analyte was allowed time to adsorb to the FOC substrate before analysis was taken. For the case of dried films, both concentrations were used separately. The solution was drop cast onto the surface of the FOC as stated before and dried under ambient conditions.

2.4.2 P-Aminothiophenol

P-Aminothiophenol (p-ATP) is an analyte that was previously demonstrated to show good surface-enhanced Raman signal with the use of gold nanoparticles[2]. Gold nanoparticles were first adsorbed to the surface of the FOC using the gold seed mediated growth process. The FOC was submerged in a 2 mM ethanol solution of the p-ATP,

covered and left overnight to ensure optimal adsorption to the Au nanoparticles. The substrate was removed, rinsed with ethanol, and dried under a nitrogen flow.

2.4.3 Carbon-Coated Copper Nanoparticles

Decoration of the FOC surface with carbon coated copper nanoparticles (CCuNP) began with the steps outlined in Section 2.3 for the samples grown on a Si-wafer substrate. The Si-wafer was placed in a beaker with 10 drops of high grade isopropanol (IPA) (99% purity, Sigma Aldrich) cast onto the surface with CCuNP. The addition of any more solvent would dilute the concentration of the CCuNP and compromise the collection of as many nanoparticles as possible in the final step. The beaker was sonicated for approximately 10 minutes to loosen the nanoparticles from the substrate. Sonicating for longer periods of time will result in degradation of the nanoparticles.

The CCuNP mixture was piped from the beaker and drop cast onto the surface of the FOC along the exposed core of the fiber. The IPA was allowed to evaporate leaving a thin film of the concentrated analyte dried to the FOC substrate for analysis.

2.5 Methods of Characterization

2.5.1 TEM

Transmission electron microscopy (TEM) images were used to characterize tomography of substrates on the nanometer scale. Additionally, the TEM machine (HR FEG-TEM/STEM) was used to determine certain chemical information about the sample using electron dispersive X-ray analysis (EDXA).

2.5.2 SEM

Scanning electron microscopy (SEM) was used to image substrates and nanoparticles. The SEM images were taken using two standard machines, Zeiss Supra

35VP and EVO 40. These machines were able to achieve images up to a 20nm resolution. The contrast created by conductivity variations in the material allowed for imaging beyond the depth of the surface.

2.5.3 Raman Spectra

All measurements referred to in this paper as being captured using a conventional Raman machine were taken using the Renishaw Invia Micro Raman spectroscopic system. This device used a red He-Ne 633 nm wavelength beam to excite the Raman transitions, with a laser power that could reach 7 mW. The Renishaw was calibrated using the central peak of a Si-wafer. An 1800 grooves/mm grating was used for resolving collected signal. Measurements were taken over areas of 10 microns in diameter.

2.6 Optical Setup

2.6.1 Data Acquisition

The collected signal was sent from the experimental set-up to the data acquisition system through an optical fiber. Upon exiting the fiber, the signal was passed through a collimating lens (Melles Griot 01LUP003). A 633nm notch filter (Semrock NF03-633E-25), with OD 6.0 and bandwidth of 25nm, was placed in the collimated beam path to extract as much of the initial laser beam as possible. The beam was then focused through a cylindrical lens (Melles Griot 01LQC004) incident upon a diffraction grating within the spectrograph (Princeton Instruments SP 2300i). For Raman measurements, a 1200 grooves/mm grating was used. This groove density allowed for fine enough resolution (FWHM 0.09 nm) of the spectrum to capture the Raman signal, yet only allowed for approximately a 40 nm range to be collected at one time. For fluorescence measurements a 150 grooves/mm grating was used, sacrificing resolution in order to collect a larger

spectral range. Finally, a charge-coupled device (CCD) was used to collect the spectral data. The cooled CCD array detector (Princeton Instruments Pixis 400) then sent the converted signal to the data acquisition software (SpectraSense) on a standard computer.

Although the bulk of the recorded measurements were collected with the CCD, occasionally an Optical Spectrum Analyzer (OSA) was used to verify results. In this case the fiber was taken directly to the OSA (Ando AQ-6315A), bypassing the data acquisition system just mentioned. The OSA, however, did not achieve the sensitivity of the CCD and therefore could not be used to collect Raman signal.

2.6.2 Absorbance Measurements

Absorbance data was taken using a broadband white light source (Phillips Focusline 6V) as a measure of whether or not the analyte was immobilized on the surface of the fiber. The light was focused into the FOC and passed through to the data acquisition set-up. In this case the notch filter was not necessary and was removed. First, the intensity of the light as a function of wavelength was collected with no analyte present. Then the analyte was drop cast onto the FOC and allowed to dry. Data again was collected for the same period of time and under the same conditions. The absorbance was calculated by taking the negative log of the ratio of these intensities.

$$(7) \quad A = -\log_{10} \left(\frac{I}{I_0} \right)$$

For analytes in solution, the respective solvent was first drop cast onto the substrate and intensity data was collected. The analyte was then added to the solvent and allowed to adsorb to the FOC surface. Alternatively, the solvent was removed entirely and a pre-mixed solution was drop cast onto the surface of the FOC, still allowing time

for adsorption to the surface. In either case, the data collected with only the solvent present was used as the initial intensity, I_0 .

2.6.3 De-coupled Measurements

2.6.3.1 Overview

It needed to be shown that the FOC could both excite Raman-active molecules and collect Raman scattering. The two processes were decoupled and checked for separately using the following set-ups. The excitation scheme passed laser light through the FOC to excite an analyte on the surface. External optical components, mounted over the active surface of the FOC, were used to collect any emission that occurred. For the collection scheme, external optical components were used to focus the beam onto the analyte on the surface of the exposed fiber. The emitted signal was then collected through guided modes in the FOC.

2.6.3.2 Excitation Scheme

The laser used in this set-up was a 632.8nm wavelength He-Ne laser (Thorlabs HRP120). In the interest of avoiding power losses, as few mirrors as possible were used to direct the beam. Preference was given to dielectric versus aluminum mirrors as they carry less loss at 633 nm. The beam first passed through a laser line filter (Thorlabs FL632.8-10-1) since the He-Ne laser beam was found to have substantial peaks in its profile outside of 633 nm. The beam was then focused into a fiber patch cable using an achromatic doublet lens (Thorlabs) of appropriate focal length to match the numerical aperture of the fiber. The patch cable was made with the same fiber as the FOC, a 0.22 NA multimode step index fiber (Thorlabs AFS50/100Y). The laser power was measured at the end of the patch cable, and generally fell between 5.5-6.0 mW. From here the laser

light was coupled into the FOC and terminated in a beaker of water to minimize reflections. The signal, fluorescence or Raman, needed to be collected along the length of the exposed fiber of the FOC. A cylindrical lens was chosen to collect a strip of light, followed by a collimating lens (Thorlabs F220-FC) that coupled the signal into a 0.37 NA step-index multimode fiber, with a core diameter of $600\mu\text{m}$ (BFL37-600). This fiber carried the signal directly to the data acquisition set-up as outlined in Section 2.6.1 where the beam would first pass through a notch filter before entering the CCD. The system was optimized by replacing the notch filter with a neutral density filter of OD 2.0 or higher, centering the grating on 633 nm, and manipulating the optics until the 633 peak was maximized.

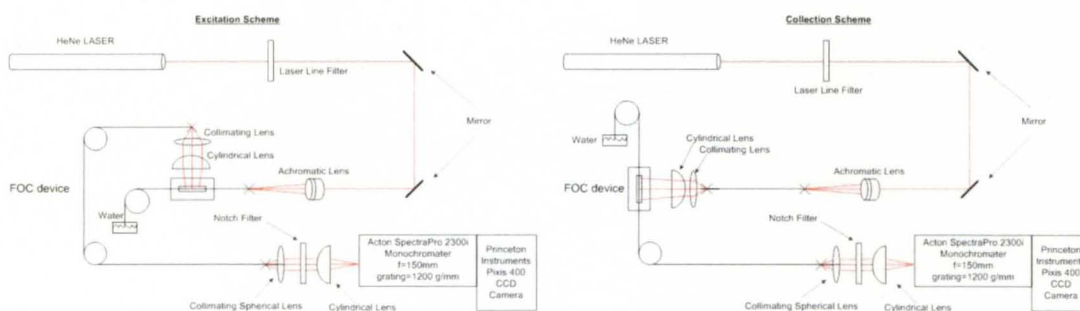


Figure 2-4 The experimental set-up for the excitation scheme in which the light is delivered to the analyte by evanescent waves (left) and the collection scheme (right) in which the light is directly focused on the FOC

2.6.3.3 Collection Scheme

Similar to the excitation scheme, the 632.8nm wavelength laser-beam passed through a laser line filter before being focused by an achromatic lens. Two set-ups were utilized in the collection scheme. The first directly focused the beam through the achromatic lens onto the FOC surface where analyte had been deposited. Only a small amount of the possible active area of the fiber was interrogated by this method.

Alternatively, the impinging laser light on the FOC could be formed into a strip that covered a greater portion of the exposed fiber. In this set-up the achromatic lens focused the light into a fiber. Differing from the excitation scheme, this time the fiber used was a 0.37 NA, 600 μm , multimode step index fiber that carried the light to a collimating lens. The collimated beam then passed through a cylindrical lens, forming a strip of light. This strip was aligned along the length of the exposed fiber of the FOC where analyte had been deposited.

In both cases, the light interacted with the analyte, creating a signal that was coupled into the FOC. One end of the FOC was deposited in a water dump to minimize reflections, while the other end carried the signal to the data acquisition set-up. Like the excitation scheme, this system was optimized by replacing the notch filter with a neutral density filter and maximizing the 633 nm peak by manipulating optics in the set-up. Figure 2-4 illustrates both the excitation scheme and the collection scheme. The only variation between the two set-ups is the way the light is delivered to the FOC and by which device the scattered light is collected.

2.6.3.4 Fluorescence Measurements

To exhibit that the optical set-up was sound and to ensure that the signal would be properly detected, the signal of a known fluorescing analyte was checked using both the excitation and collection schemes. Previous work in our lab has shown bovine serum albumin (BSA) to be an analyte that demonstrates successful fluorescence measurements using the FOC device. As such it was chosen as the testing analyte. The grating used in these experiments was the 150 grooves/mm. The cylindrical lens set-up was used in the

excitation scheme, exciting across the length of the fiber rather than focusing on a single point.

For both the excitation and collection set-ups, a buffer was first drop-cast onto the surface of the chip and data was collected. The BSA was then added to the buffer and allowed to incubate for 10 minutes to ensure that it adsorbed to the surface. Data was then collected for the same time duration and under the same conditions as when the buffer alone was present. The buffer data was treated as background and subtracted out.

2.6.4 Fully Guided System

2.6.4.1 Overview

The overarching goal of the project was to combine the collection and excitation schemes to a fully integrated system using minimal bench top optical components. The fully guided system required only that light be coupled into the FOC. Light from a He-Ne laser at 632.8 nm was first directed through a laser line filter to an achromatic lens. The light was then focused and coupled into a patch cable of the same fiber composition as the FOC. This fiber was used to deliver the light to the fully guided system. At the end of this fiber is where power was monitored. The light would pass through the FOC, interacting with the analyte adsorbed to the surface. The signal from the analyte would then be directed into the FOC through near-field coupling. The signal would then travel through the FOC to the data acquisition set-up where the exciting light would be subtracted or removed.

2.6.4.2 Inline Coupler

An inline optical coupler (Thorlabs FCMM625-99A-FC) was used for one iteration of the fully guided system set-up. It was a three-port system. In this scheme,

light was coupled into one port of the coupler and through another port sent to the FOC. The light would pass through the FOC, interacting with the analyte, and then terminate in a beaker of water to minimize back reflections. The signal from the FOC would emerge in both directions, both terminating in water and moving through the port that the initial laser beam traveled through. The signal from the FOC was not split evenly between the two other ports; 1% was sent in the direction of the initial light source. The remaining 99% was sent to the data acquisition system. This set-up allowed for less of the exciting beam to reach the data acquisition system.

2.6.4.3 Annular Mask Experiment

To alleviate the lower order modes that did not interact with the surface of the substrate an annular mask was used [45]. This mask allowed only a thin shell of the outer most modes of a collimated beam to be coupled into the fiber as demonstrated in Figure 2-5. It was important that the fiber's radius of curvature remain small to ensure the modes did not scramble from this point.

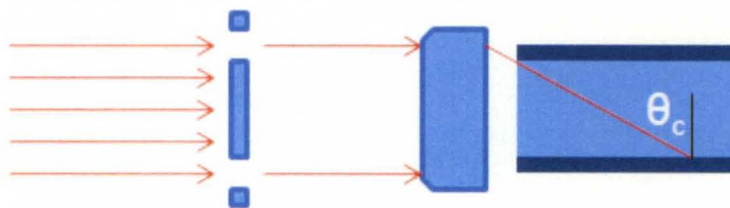


Figure 2-5 A side view of the annular mask. Only light passing through the slit of the mask will be guided into the fiber, only allowing for higher order modes that will have increased interaction with the analyte.

The mask was created by punching out a hole from a piece of black plastic. The punch-out was adhered to a microscope slide using a two part epoxy (Epotek 301). A hole of larger size was centered around the punch-out and secured using electrical tape.

The beam was collimated and then coupled in the FOC using an optical U-bench

(Thorlabs FB240FC). The collimating lenses housed in the U-bench were 0.5NA with a focal length of 8 mm. The mask was centered in the collimated beam path, allowing only a ring of light to enter the second collimated lens and couple into the FOC.

2.6.4.4 Higher-Index Capping Layer

For this experiment, the optical gel (Cargille) was deposited in a thin, even layer across the active area of the FOC. Care was taken that no air bubbles were created in the bulk of the medium. The optical gel was drop cast on both an FOC with the Raman active analyte and on a bare FOC. Investigations were made using the excitation scheme detailed in this chapter, and a fully integrated set-up. For the fully integrated approach, the exciting laser beam was coupled into the FOC directly without the use of any additional fibers to guide the beam in an effort to cut down on as much fluorescent background as possible. The Raman signal was collected by the FOC and guided to the data acquisition set-up.

CHAPTER 3: RESULTS AND DISCUSSION

3.1 Preliminary Work

The fiber optic chip (FOC) has undergone some modifications in its fabrication process since the first generation device was created at the University of Arizona. Variations include a more stable polishing console which ensures even removal of the cladding and an etched Si-wafer replaced a glass V-groove. A deeper tapered mount is now used to inhibit breakage of the fiber at the cladding interface, but as a result the path length has been slightly lessened.

Fluorescence measurements were collected using bovine serum albumin (BSA) to verify that the utility of this device was maintained after these modifications as well as to test the set-up of the beam steering optics and data acquisition equipment to be used. The excitation and collection schemes were tested separately as described in Chapter 2. Impinging laser light was used to excite emission from adsorbates on the FOC. For the excitation scheme, the light was delivered to the analyte by the FOC and the scattered emission was collected by external optical components mounted above the FOC. For the collection scheme, light was focused on the surface of the FOC by external optical components and the emitted signal of the analyte was collected by the FOC and sent to the data acquisition system. For each set-up, first signal from the buffer was collected. To the buffer was added the BSA and 10 min was given to allow the analyte to adsorb to the surface of the FOC. Then signal was collected from the BSA solution for the same

amount of time and under the same conditions as the buffer alone. The buffer signal in the excitation and collection schemes was treated as background and subtracted from the respective BSA data. Fluorescence was seen from an exciting wavelength of 632.8 nm

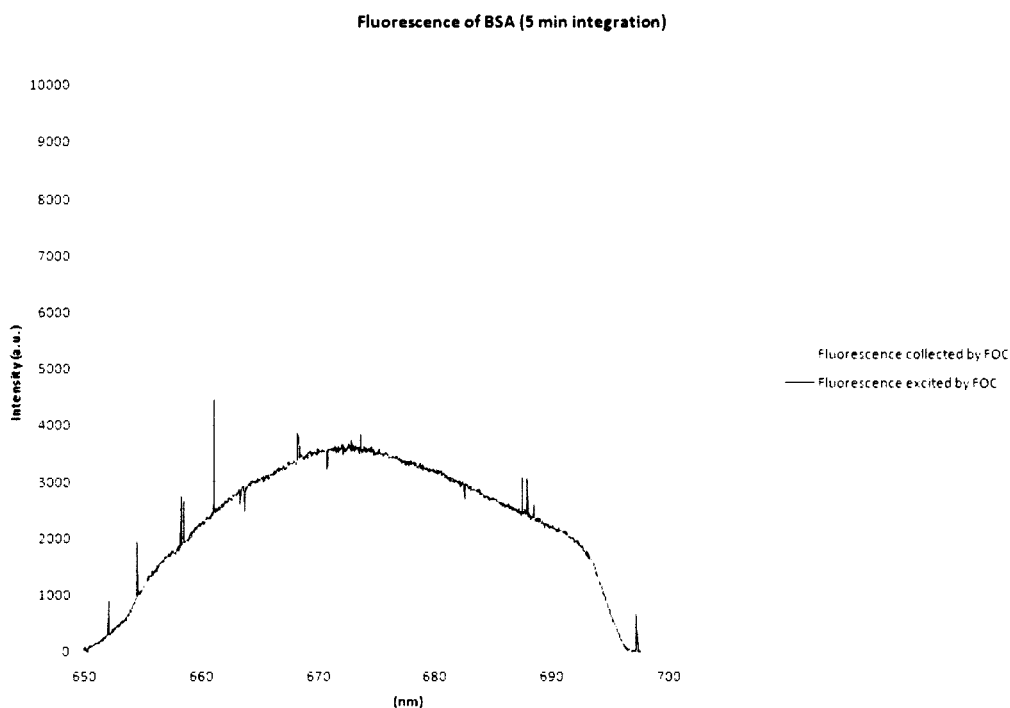


Figure 3-1 Fluorescence data of the BSA analyte for both the collection and excitation schemes using the FOC.

over a 5 min time exposure (See Figure 3.1). This proof of concept confirmed the viability of the optical set-up and FOC fabrication.

3.2 Rhodamine-6G Experiments

Rhodamine-6G (R6G) is a Raman-active analyte used in dye lasers as the gain medium. For these experiments, a 1mM aqueous solution of R6G was prepared. To demonstrate R6G was adsorbing to the surface of the FOC and interacting with the excitation light, absorbance data was taken using a white light source. De-ionized water

was used as the initial intensity in the absorbance equation as the R6G was analyzed in aqueous solution. The optical spectra (see Figure 3-2) matched data from an online database provided by the Oregon Medical Laser Center and provided evidence that the light traveling through the fiber was being attenuated by the R6G analyte adsorbed to the FOC surface.

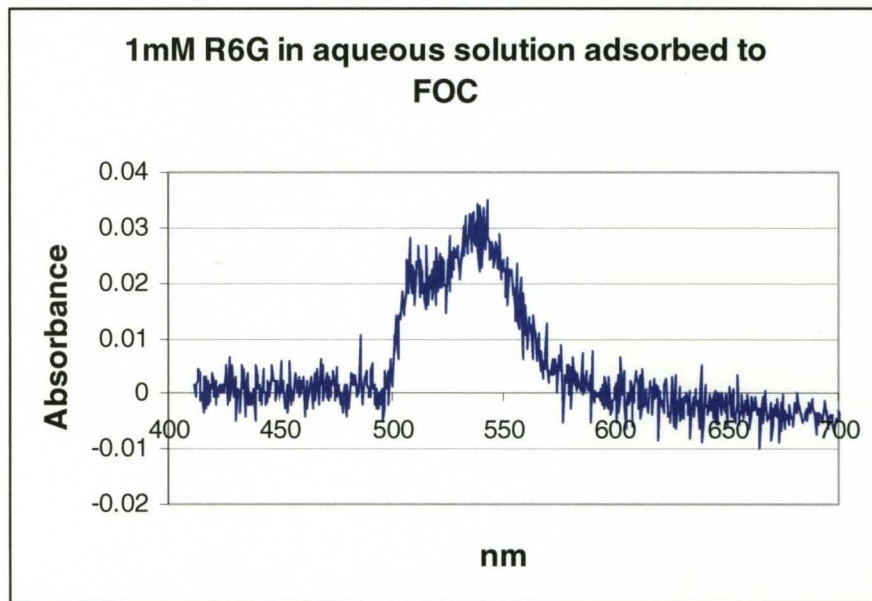


Figure 3-2 Absorbance data of Rhodamine-6G using a white light source and collecting signal with the inline configuration.

The next step was to test for Raman signal from the R6G analyte. First the excitation scheme through guided modes in the FOC was investigated, and emission signal was collected through a cylindrical lens. Again, DI-water alone was used as a background, interrogated under the same circumstances as the R6G and subtracted from the raw R6G data. The same process was carried out for the collection scheme through guided modes in the FOC and excitation with external optical components. In both cases, no signal was seen. In an effort to excite the Raman-active analyte, power of the system

was optimized through optical alignment. Already data had been collected for 30 min intervals, so elongating the integration time was not as viable an option without compromising the data due to cosmic ray noise. Despite improvements in alignment, still no Raman signature of the R6G analyte was detected.

As a final step to generating Raman scattering, the analyte was allowed to dry on the FOC. This thin film was much more concentrated than the adsorbed layer of the aqueous solution and therefore the cross-section of Raman interaction would likely increase. Acting as the background to be subtracted from the dried R6G raw data was ambient air. A decided increase in signal was collected, however the features were broad and likely corresponded to the large fluorescence generated by R6G. Figure 3-3

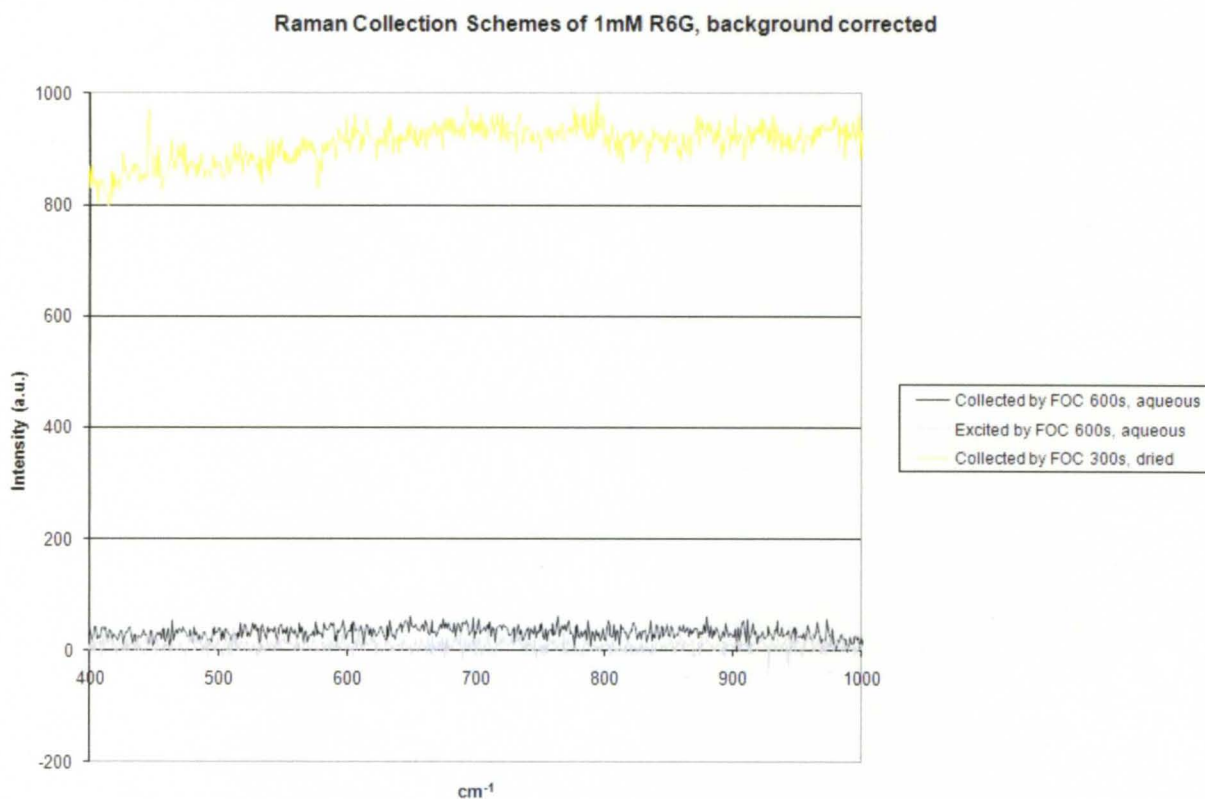


Figure 3-3 Data collected from the FOC with the R6G analyte for 600s intervals, excited by a 633nm wavelength.

illustrates the feature-less signal of the R6G under both aqueous and dried conditions.

Due to the absence of Raman emission from the collected spectra of the R6G analyte, a second analyte was investigated. Single walled carbon nanotubes (SWNT) were probed under the same conditions as the R6G. SWNT have a distinct Raman signature and this particular sample was first tested in a conventional Raman machine for Raman activity. Once it was verified that the SWNT were Raman-active, they were deposited on the FOC using an isopropanol (IPA) solution and excitation and collection were attempted. Secondly, the IPA was allowed to evaporate and the SWNT were interrogated as a thin film. In both cases, no Raman activity was seen, possibly as a result of increased scattering due to the macroscopic geometry of the sample.

3.3 Surface Enhancement of FOC

As reported in the literature, surface-adsorbed R6G only produces a small signal and typically requires plasmonic enhancement on the surface to produce a reasonable emission spectrum. To address this issue, we have been working with Dr. Zamborini of the University of Louisville Chemistry Department to functionalize the surface of the FOC with gold nanoparticles (AuNP). Gold was chosen due to its stability under ambient conditions for a longer duration when compared with silver. The surface of the FOC was functionalized with mercaptopropyltrimethoxysilane (MPTMS) to which the AuNP were adsorbed. Details of the gold seed mediated growth process, which produces nanospheres, rods, and platelets, can be found in Chapter 2.

Because the exact adsorption rate of R6G to the AuNP was unknown, the analyte 4-aminothiophenol (p-ATP) was chosen instead as there was published work on its Raman activity in the presence of gold [46]. In addition, all of the Raman peaks of p-ATP

occur within a range of 30 nm when excited by a 633-nm wavelength. Unlike previous analytes investigated, this meant that the entire Raman spectrum could be collected without moving the grating of the spectrograph such that data would not have to be parsed together.

Exciting through the fiber, Raman peaks of the p-ATP analyte were collected over Exciting and 10 minute integration times to achieve acceptable SNR. It should be noted that collecting background data from the FOC without the analyte was not desirable as the adsorption of the analyte was an overnight process and changes could occur in the optical set-up environment, such as power fluctuations in the light source. No background data could be taken after the Raman data was collected without permanently removing the analyte and AuNP. If the FOC was to be functionalized for SERS again the entire AuNP growth process would have to be repeated. This process involves submersion in solvents for long periods which proved to be harmful to the integrity and lifetime of the FOC. Therefore the background data for these experiments measured only the dark signal of the detector and any stray light that was able to reach the detector.

The expected Raman shift spectrum from the enhanced p-ATP analyte appears in Figure 3-4. This Figure contains spectra from both an outside source under similar enhancement conditions and data collected from the FOC by a conventional Raman machine (Renishaw Invia). As the image labeled *Excitation Scheme* of Figure 3-5 shows, the Raman signal of the p-ATP analyte was excited by the FOC. The Raman emission generated by the FOC was collected by external optical components. The peaks from the excitation scheme match well with Figure 3-4, demonstrating the ability of the FOC to

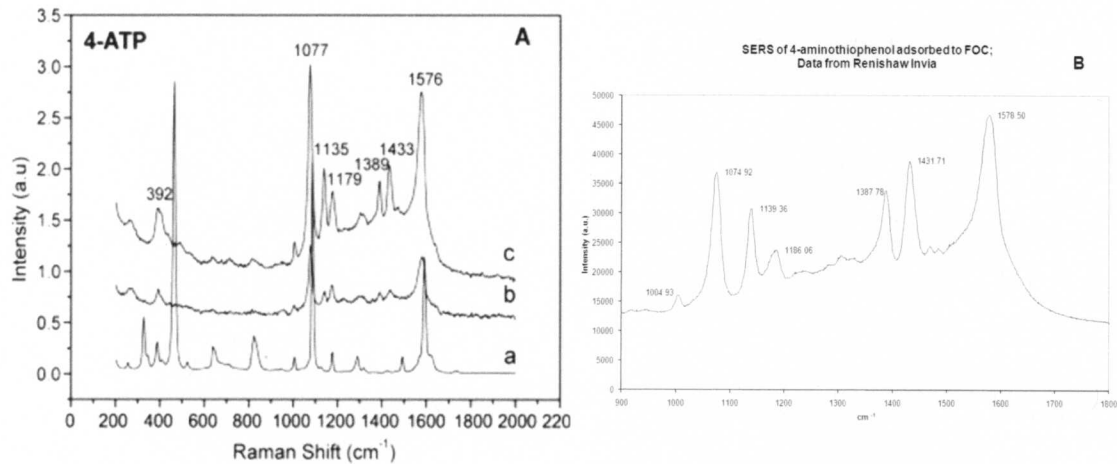


Figure 3-4 Raman spectra of 4-aminothiophenol analyte as collected by [A] Wang et. al.[2] without enhancement (a), with evenly distribute gold nanoparticles (b), and with aggregated gold nanoparticles (c); and [B] by Renishaw Invia from functionalized FOC.

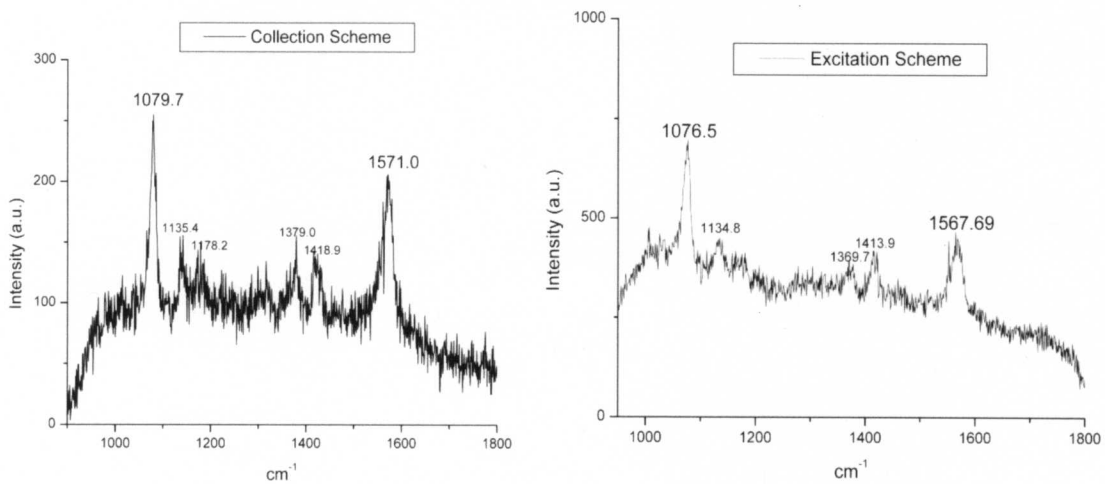


Figure 3-5 Raman signal from p-ATP analyte when being excited by an outside source and collected through the FOC (left), and when generated by the FOC and collected by bench-top optical set-up

generate emission spectra comparable to well-established modalities of Raman signal collection.

Once the excitation of the p-ATP was shown be successful using the FOC, the collection of the Raman signal by the FOC was attempted. The analyte was excited by external optical components, and the p-ATP Raman signal was successfully collected by the FOC and propagated to the data-acquisition system. Again referring to Figure 3-5, the

image labeled *Collection Scheme* shows the Raman spectrum of p-ATP in very good agreement with the data of the conventionally collected signal as well as the excitation scheme. This demonstrates the feasibility of the device to collect and carry the Raman signal through the fiber when the analyte is excited remotely.

It is interesting to note that collection of the Raman signal through the fiber was not as readily achieved as excitation by the FOC. To attain similar peak heights, the integration time was extended to 20 min. To demonstrate simply that the fiber was capable of coupling the Raman signal, the exciting light was focused onto a single point of the fiber active area rather than a strip of light across the entire path length. To ensure consistency, several points across the fiber were excited separately and compared.

Growth times were varied for three different FOC devices such that AuNP diameters were 5 nm, 10 nm, and 20 nm respectively. Enhancement was strongest for the 20 nm case, however growth beyond this size was not considered since the analyte needs to be close to the surface of the FOC to undergo evanescent field excitation.

Additionally, the intensity of the Raman signal was monitored as a function of power. It was shown that with as little as 0.6mw of power supplied to the FOC, the analyte was still detected as seen in Figure 3-6. Excitation from lower power could potentially be generated and detected by elongating the exposure time, however the potential for system fluctuations would increase.

3.4 Fully-Guided Raman Detection

3.4.1 Initial Experiment

The next step was to show that the Raman signal could be both excited by the FOC and coupled back into the FOC for collection, creating a fully in-line system. For this experiment, only beam steering optics were needed to focus the incident laser beam into the fiber and direct the subsequent Raman signal to the detector. For the in-line

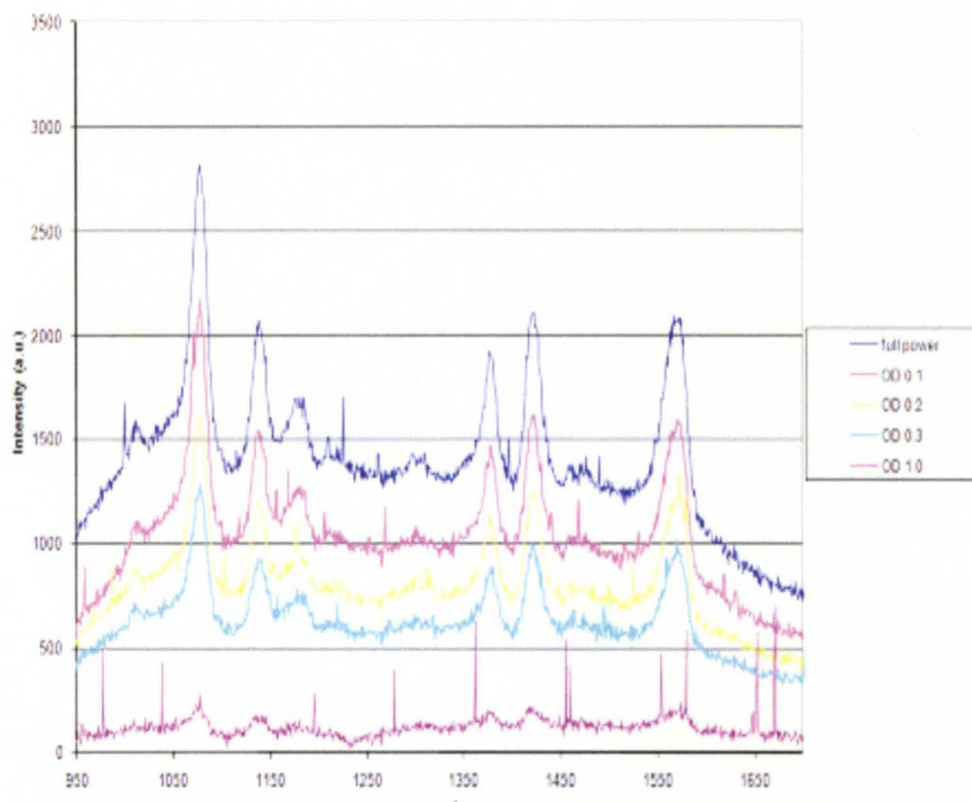


Figure 3-6 Raman scattering intensity of p-ATP as a function of power level. Initial power was measured at 6mW.

experiment, only very short integration times, 50 ms to 5 s, were achievable before the CCD was saturated. This effect was not expected as neither the excitation or the collection data had very high levels of overall intensity. Previous data showed that the Raman signal was still generated even with lower power supplied to the FOC. The initial

power was reduced using a neutral density filter, yet the intense background shape remained with no additional Raman peaks. The broad peak suggested fluorescence was being generated either by the analyte or the fiber itself. The FOC was removed from the system and replaced by a patch cable composed of the same fiber used in the FOC. Again the signal was quite large, alleviating the possibility that there was a background fluorescence caused by the analyte. It was possible that the background was only the shoulder of a broad laser profile that was being transmitted through the fiber. To test this, a laser line filter was placed in the beam path before the laser line entered the fiber allowing only the 633-nm wavelength to pass. Again, the same intense, broad background was generated. This suggested that the source of the fluorescing was limited to the fiber and created a background that was stronger than any signal coming from the analyte.

After determining that the fiber itself was fluorescing, consideration needed to be given as to why the fluorescence had not been seen until now. Through TIR, the fluorescence was not escaping the fiber therefore it was not detected in the excitation scheme. For the collection scheme, then intense laser beam was not traveling the entire length of the fiber and therefore did not generate as much fluorescence.

Literature supports this assumption, as fluorescing and stray Raman peaks generated by optical fibers have been a hurdle for the development of fiber optic probes, requiring creative filtering mechanisms or use of a longer wavelength excitation beam [47].

3.4.2 Modifications to Alleviate Fluorescence

The initial approach to overcome the difficulties above was to try another fiber, one that was UV transparent and potentially would not fluoresce in the visible region. Unfortunately, due perhaps in part to absorption by unknown dopants in the fiber, the fluorescence background was actually higher for the UV fiber.

As mentioned in the introduction of this paper, the phenomenon of anti-Stokes (AS) Raman scattering occurs when the analyte is already in vibrationally excited state and imparts some energy to the impinging photon. The AS Raman peaks are blue shifted from the exciting wavelength rather than red shifted. Because this places the Raman activity in a quieter area of the spectrum, it was thought to be advantageous to probe AS scattering for the p-ATP analyte. If the analyte does not demonstrate AS scattering at room temperature, it may need to be heated to excite the molecules into a higher vibrational state. Other groups have demonstrated AS when heating an analyte up to 350 °K [48]. The drawback is that the current materials used in the FOC cannot withstand temperatures much higher than 90°C, the temperature at which the epoxy is cured. Prior to heating the FOC, a piece of Si-wafer used as a control in the AuNP growth process was functionalized with the p-ATP analyte. Using a hot plate in a conventional Raman machine, temperatures were increased well past 100°C and still no p-ATP AS scattering was seen, although the Si-wafer AS peak was generated. Unfortunately, this result determined that AS scattering could not be used to bypass the fluorescing of the fiber.

The surface-adsorbed analyte interacts more with higher order modes of the optical fiber as they have stronger electromagnetic field intensity and impinge on the interface of the core boundary with greater frequency, while lower order modes largely

remain confined to the center of the fiber and likely create the majority of the fluorescing. An annular mask was developed to block lower order modes from propagating through the fiber. In this experiment, an interruption was created in the fiber beam path and the annular mask was inserted just before interactions with the analyte. A fiber delivered the exciting light to a collimating lens on an optical U-bench mount. The collimated beam passed through the annular mask and only a ring of the initial light was allowed through.

$r_{out} = 3.52 \text{ mm}$ $A_{out} = 38.93 \text{ mm}^2$		
$r_i \text{ (mm)}$	$A_i \text{ (mm}^2\text{)}$	A_{i-g} / A_{out}
3.18	31.77	0.18
2.78	24.28	0.38
2.38	17.80	0.54

Table 1 Calculating the percentage of the initial beam diameter that remained after installation of annular mask.

The light was then focused back into the fiber and passed through the FOC in an in-line configuration. The size of the outer diameter of

annular mask was chosen based on the beam size as determined by the NA of the fiber and the lenses in the U-bench set-up. A number of prefabricated punch-outs of smaller diameter were centered inside the outer diameter to block a particular percentage of the incoming light. The effect was only an attenuated of the overall fluorescent signal, although some irregular features were noticed on the curve they were present even when the analyte was not.

After reviewing the data of the Raman active analyte, it became clear that the FOC device was weaker at coupling the Raman signal than it was at exciting it. The result was a poor signal to noise ratio (SNR) due to the inherent fluorescence of the fiber. The core of the optical fiber used in the FOC carried an index of refraction at 633 nm of 1.457. In order to maintain TIR, bulk medium deposited on the exposed core must have

an index of refraction which is lower than this. For thin films such as the p-ATP, ambient air serves this purpose. If instead a homogenous dielectric medium of refractive index was placed on top of the analyte, excitation signal as well as previously generated fiber fluorescence would be effectively pulled out of the fiber. Rather than devise a mechanism to improve the near field coupling, a layer of a medium with higher refractive index than that of the fiber was deposited to the FOC active area. This increase in index of refraction would lead to a disruption in the total internal reflection and allow both the exciting wavelength and the fluorescence to escape the fiber along the D-shape path. Because for unpolarized light the Raman scattering direction is random, this would not have an effect on coupling the Raman signal of the analytes adsorbed very close to the boundary of the core. The effect would be a decrease in fluorescence generated before the FOC as well as a reduction of the initial laser beam passing through the fiber between the analyte and the detector, reducing fluorescence produced in this region of the fiber. This would effectively improve the SNR of the signal collected through the fiber.

The bulk medium chosen for this experiment was a commercial optical gel (Cargille 081160) with $n = 1.514$ at 633nm. The data was collected using the fully-guided set-up as before, this time with the capping layer of the optical gel. With the optical gel in place, the saturation point of the CCD was not reached when collecting for the same amount of time. Although a reduction in overall fluorescing was obtained, Raman signal was not resolved in the spectra gathered from the in-line set-up with the addition of the optical gel.

When a higher indexed medium is used reflections will still occur at the boundary of the index change, so not all of the fluorescence and exciting light would be removed.

However, if a capping layer of matching refractive index was deposited on the analyte the light would continue to pass through the medium as if it were the core, effectively removing a significant amount of the fluorescing as well as the incident laser light and thus improving SNR. To further exploit the ability of the optical gel to reduce fluorescence, another optical gel (Cargille 0607) of very close refractive index to the core, $n = 1.456$, was deposited on top of the SERS activated p-ATP on the FOC. Again, the fluorescent background was effectively reduced, yet no Raman features could be resolved from the fully guided spectra.

To ensure that Raman signal was being generated by the FOC and simply not being detected by the fully-guided set-up, external optics were mounted above the FOC and collected the signal of the p-ATP covered by the optical gel. The resultant spectra showed that Raman signal was being generated by both the p-ATP analyte and the optical gel. To further probe this fact, the optical gel was examined in the excitation scheme without the p-ATP or the presence of AuNP. It was found that the optical gel itself had Raman features which were very strong when signal was collected via the excitation scheme without the addition of AuNP as seen in Figure 3-7. This served as a demonstration that the FOC may be used to excite bulk material without SERS.

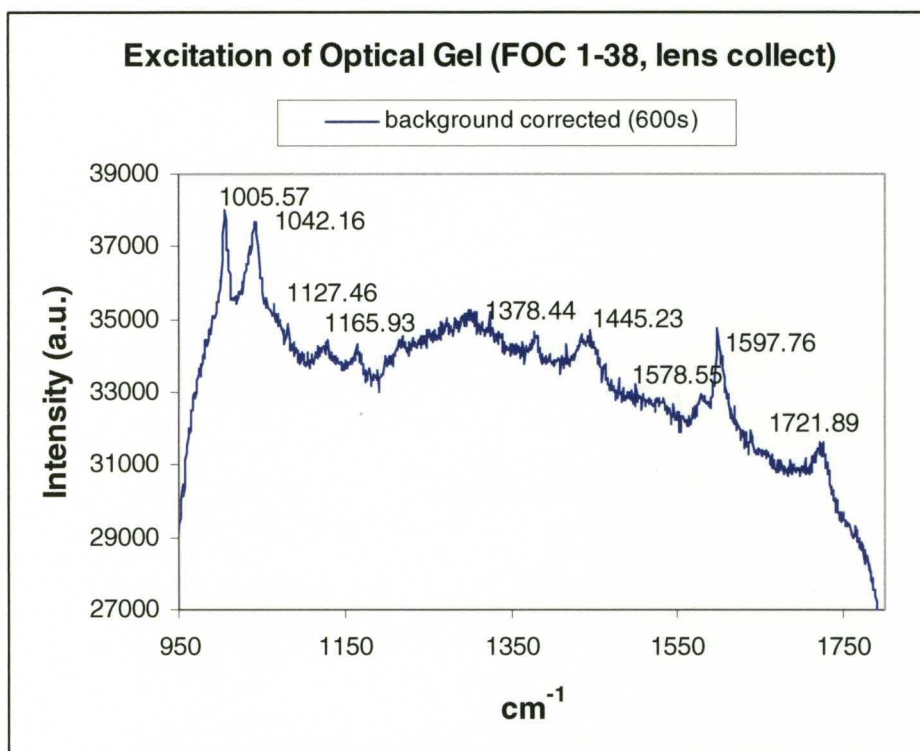


Figure 3-7 Raman signal of optical gel generated by FOC.

3.5 Carbon-Coated Copper Nanoparticle Experiment

An adjunct project to probing Raman scattering abilities of the FOC was to produce a functionalizing agent using graphene for future investigations. As mentioned previously, graphene demonstrates promise as a sensor due to its conductivity. Resistance variation in the presence of analytes has been discussed in this paper so a graphene substrate may be paired with the FOC to offer some information about an analyte or environment. To bolster the analytical properties of this sensing mechanism, we paired a nanoparticle substrate to make use of localized surface plasmon effects in the vicinity of an electromagnetic field.

For this project, a thin film of Cu was deposited on a Si-wafer substrate. By a CVD growth process, graphene was deposited on top of the Cu layer. The Cu-film disassembled into particle aggregations under the conditions of the CVD furnace and were encapsulated by the graphene layer. Variations were made to construct a consistent size and shape suitable for use with the FOC. Additionally, manipulations were made on the growth process to develop monolayer and multiple layer graphene as well as carbon nanotubes. The conditions under which the best growth was achieved involved a 1 – 5 nm Cu thin film layer, a 3 – 4 minute growth process, and a ramping of the temperature from

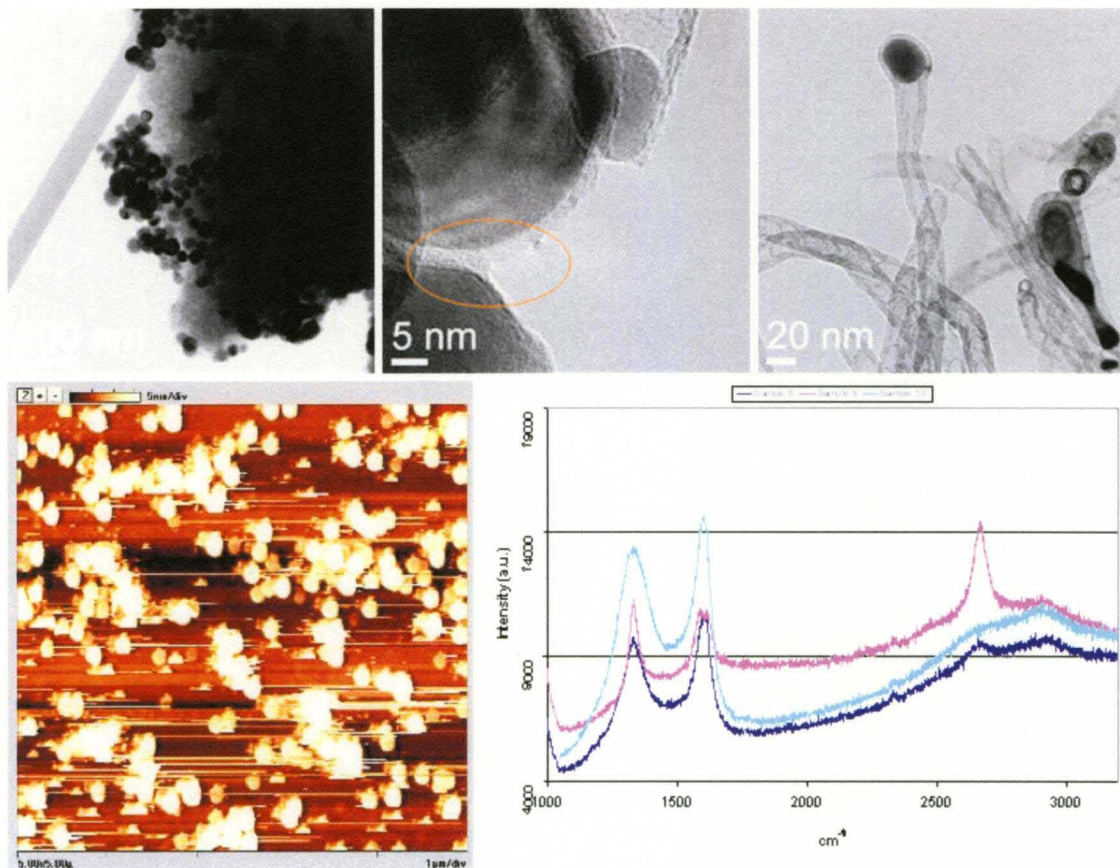


Figure 3-8 Clockwise from top left: C-coated Cu nanoparticles dispersed in amorphous carbon; multi-layer graphene encapsulating Cu nanospheres; C-nanotubes growing from CuNP; Raman spectra of CCuNP; AFM image of Si-wafer substrate decorated with CCuNP.

0 to 300 to 900 °C. As seen in Figure 3-8, images taken by TEM and AFM machines reveal the consistency of the nanoparticles size and shape, however amorphous carbon and nanotubes are formed in addition to the desired CCuNP. The temperature-ramping seemed to have the greatest effect on the consistency of the size and shape of the nanoparticles. Growth time and Cu thickness determined the ratio of graphene to carbon. Too long of a growth period or thin of a layer of Cu and the CCuNP would be found in a sea of amorphous carbon.

It should be noted that attempts were made to detect the CCuNP using the FOC as described in Section 2.4.3, however very few of the nanoparticles remained on the substrate after TEM analysis. Transferring the CCuNP to the FOC left even less to sample, therefore Raman signal from the CCuNP was not generated or collected by the FOC.

CHAPTER 4: CONCLUSIONS AND OUTLOOK

4.1 Conclusions

The work of this project has demonstrated the ability of the FOC to generate as well as couple Raman scattering for thin films and bulk media. The device itself boasts many attributes. Its portability is inherent to optical fiber devices, but additionally the absence of need for a high voltage power supply, cooling lines, or a vacuum system allow this platform to be quite mobile when compared with other analytical techniques. The side-polished geometry allows for easier control of surface chemistry and a solid platform for analyte deposition. Successful protocols have been established for functionalizing the surface for SERS experiments and give promise to future surface functionalization. Additionally, the extended path length of the D-shape when compared to other Raman fiber-optic probe designs allows for a larger cross section of analyte signal coupling as well as takes advantage of evanescent field mechanisms freeing the user of the need for optical alignment.

Through its increased utility and fully guided design, the FOC is on route to becoming a stand-alone device for wide-spread use. Much work still needs to be done to fully realize this objective, however the work presented here has set a foundation for future investigations and modifications.

4.2 Future Work

Continuation of this project will confront the issue of fluorescence in the fiber as this is the main obstacle for a fully guided device. Potentially, the exciting wavelength could be changed to a longer wavelength to reduce the fluorescing due to the fiber. Commercially available fibers have greater transmission in the IR region of the spectrum suggesting excited fluorescence would be nominal. Little will need to be done to alter the current optical set-up as we have available a tunable pulsed laser (Panther) which can easily achieve lasing up to the micron level. However, the CCD detector in use does not have the capacity to collect data from this region of the electromagnetic spectrum, therefore different acquisition set-up would need to be put in place.

Anti-Stokes measurements were considered as a way to avoid fluorescence, but the heating of the epoxy limited the use of this mechanism. If, however, the active area of the analyte were heated locally through a probing light source, AS scattering may still be achieved without the damaging effects to the FOC infrastructure [49]. Another benefit of local heating is the potential ability for a tunable SERS substrate [50]. Spacing of metallic nanoparticles plays a key role in the enhancement factors when related to the excitation beam and index of refraction of the dielectric medium surrounding them. A thermally tunable substrate would allow for the optimized utility of SERS substrate for various exciting laser lines and interrogation of solutions with varying dielectric constants.

Another approach which focuses on the optimization of the SERS substrate would make use of the analytical and numerical models for local E-field enhancement in the region near a metallic nanoparticle, as mentioned in Section 1.1. Analytical models give

solutions of E-field enhancement for spherical and ellipsoidal nanoparticles as a function of the size of the nanoparticles as well as the frequency of the incident light. Using this model, it may be shown that for gold nanospheres having a diameter similar in size to those detailed in Section 2.2, the greatest E-field enhancement is seen for approximately a 524 nm incident wavelength. Changing the exciting wavelength from 633 nm to a wavelength closer to 524 nm may increase the overall E-field enhancement generated by the gold nanoparticles. Additionally, numerical solutions for non-spherically shaped nanoparticles suggest tremendous enhancement, up to 500 times the initial E-field intensity, at the tips of nanoplatelets. Figure 4-1 shows the E-field enhancement of a nanoplatelet as calculated using the numerical method referred to as the discrete dipole approximation (DDA), where a greater enhancement is seen for the 770 nm wavelength [11]. Future manipulations to the nanoparticle growth process to fabricate nanoplatelets and nanorods may further increase the surface enhancement already seen in the preceding experiments.

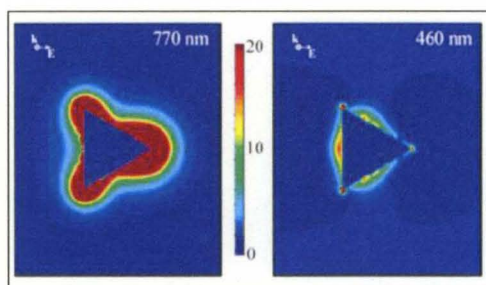


Figure 4-1 E-field enhancement as calculated by the DDA numerical method near a nanoplatelet for both 770 and 460 nm excitation wavelength [11].

Further investigation into the decoration of the FOC substrate for various applications should be pursued. A thin film deposition for SPR could readily be paired

with subsequent layers of NP for surface enhancement, creating a device that may generate and collect SPR and Raman data simultaneously. This use of electrostatically deposited graphene for possible fluorescence quenching [51] and the addition lithographic nanopillar structures for surface enhancement are two other possible avenues for future functionalization of the FOC.

REFERENCES

1. Utzinger, U. and R.R. Richards-Kortum, *Fiber optic probes for biomedical optical spectroscopy*. Journal of Biomedical Optics, 2003. **8**(1): p. 121-147.
2. Wang, Y., et al., *Facile fabrication of large area of aggregated gold nanorods film for efficient surface-enhanced Raman scattering*. Journal of Colloid and Interface Science, 2008. **318**(1): p. 82-87.
3. Smith, E. and G. Dent, eds. *Modern Raman Spectroscopy: a practical approach*. 2005, John Wiley and Sons Ltd: Chichester. 71-134.
4. Xu, Q.F., et al., *Determination of methanol ratio in methanol-doped biogasoline by a fiber Raman sensing system*. Sensors and Actuators B-Chemical, 2010. **146**(1): p. 75-78.
5. Premasiri, W.R., et al., *Characterization of the Surface Enhanced Raman Scattering (SERS) of bacteria*. Journal of Physical Chemistry B, 2005. **109**(1): p. 312-320.
6. Vo-Dinh, T., F. Yan, and M.B. Wabuyele, *Surface-enhanced Raman scattering for medical diagnostics and biological imaging*. Journal of Raman Spectroscopy, 2005. **36**(6-7): p. 640-647.
7. Kerker, M., D.S. Wang, and H. Chew, *SURFACE ENHANCED RAMAN-SCATTERING (SERS) BY MOLECULES ADSORBED AT SPHERICAL-PARTICLES*. Applied Optics, 1980. **19**(24): p. 4159-4174.
8. Felidj, N., et al., *Optimized surface-enhanced Raman scattering on gold nanoparticle arrays*. Applied Physics Letters, 2003. **82**(18): p. 3095-3097.
9. Gupta, R. and W.A. Weimer, *High enhancement factor gold films for surface enhanced Raman spectroscopy*. Chemical Physics Letters, 2003. **374**(3-4): p. 302-306.
10. Kneipp, K., et al., *Single molecule detection using surface-enhanced Raman scattering (SERS)*. Physical Review Letters, 1997. **78**(9): p. 1667-1670.
11. Kelly, K.L., et al., *The optical properties of metal nanoparticles: The influence of size, shape, and dielectric environment*. Journal of Physical Chemistry B, 2003. **107**(3): p. 668-677.
12. Noguez, C., *Surface plasmons on metal nanoparticles: The influence of shape and physical environment*. Journal of Physical Chemistry C, 2007. **111**(10): p. 3806-3819.
13. Mirabella, F.M., *INTERNAL-REFLECTION SPECTROSCOPY*. Applied Spectroscopy Reviews, 1985. **21**(1-2): p. 45-178.
14. Sohn, K.R., K.T. Kim, and J.W. Song, *Optical fiber sensor for water detection using a side-polished fiber coupler with a planar glass-overlay-waveguide*. Sensors and Actuators a-Physical, 2002. **101**(1-2): p. 137-142.

15. Smith, K.H., et al., *Versatile in-fiber sensing by use of core-replaced D-fiber*. Applied Optics, 2005. **44**(1): p. 22-26.
16. Flannery, D., et al., *Fiber-optic chemical sensing with Langmuir-Blodgett overlay waveguides*. Applied Optics, 1999. **38**(36): p. 7370-7374.
17. Carlyon, E.E., et al., *A SINGLE-MODE FIBEROPTIC EVANESCENT WAVE BIOSENSOR*. Biosensors & Bioelectronics, 1992. **7**(2): p. 141-146.
18. Tempelman, L.A., et al., *Quantitating staphylococcal enterotoxin B in diverse media using a portable fiber-optic biosensor*. Analytical Biochemistry, 1996. **233**(1): p. 50-57.
19. Gao, H.H., et al., *Tapered fiber tips for fiber optic biosensors*. Optical Engineering, 1995. **34**(12): p. 3465-3470.
20. Kang, K.A., et al., *Near real-time immuno-optical sensor for diagnosing single point mutation A model system: Sensor for factor V leiden diagnosis*. Biosensors & Bioelectronics, 2009. **24**(9): p. 2785-2790.
21. Spiker, J.O. and K.A. Kang, *Preliminary study of real-time fiber optic based protein C biosensor*. Biotechnology and Bioengineering, 1999. **66**(3): p. 158-163.
22. Potyrailo, R.A., S.E. Hobbs, and G.M. Hieftje, *Near-ultraviolet evanescent-wave absorption sensor based on a multimode optical fiber*. Analytical Chemistry, 1998. **70**(8): p. 1639-1645.
23. Poscio, P., et al., *REALIZATION OF A MINIATURIZED OPTICAL SENSOR FOR BIOMEDICAL APPLICATIONS*. Sensors and Actuators a-Physical, 1990. **23**(1-3): p. 1092-1096.
24. Huntington, S.T., et al., *Field characterization of a D-shaped optical fiber using scanning near-field optical microscopy*. Journal of Applied Physics, 1997. **82**(2): p. 510-513.
25. Lee, B., S. Roh, and J. Park, *Current status of micro- and nano-structured optical fiber sensors*. Optical Fiber Technology, 2009. **15**(3): p. 209-221.
26. Potyrailo, R.A., S.E. Hobbs, and G.M. Hieftje, *Optical waveguide sensors in analytical chemistry: today's instrumentation, applications and trends for future development*. Fresenius Journal of Analytical Chemistry, 1998. **362**(4): p. 349-373.
27. Khijwania, S.K., et al., *A fiber optic Raman sensor for hydrocarbon detection*. Sensors and Actuators B-Chemical, 2007. **125**(2): p. 563-568.
28. Lima, C.J., et al., *Catheter with dielectric optical filter deposited upon the fiber optic end for Raman in vivo biospectroscopy applications*. Spectroscopy-an International Journal, 2008. **22**(6): p. 459-466.
29. Krafft, C., et al., *Methodology for fiber-optic Raman mapping and FTIR imaging of metastases in mouse brains*. Analytical and Bioanalytical Chemistry, 2007. **389**(4): p. 1133-1142.
30. Tiwari, V.S., et al., *Fiber optic Raman sensor to monitor the concentration ratio of nitrogen and oxygen in a cryogenic mixture*. Applied Optics, 2007. **46**(16): p. 3345-3351.
31. Mo, J.H., et al., *High Wavenumber Raman Spectroscopy for in Vivo Detection of Cervical Dysplasia*. Analytical Chemistry, 2009. **81**(21): p. 8908-8915.

32. Cooney, T.F., H.T. Skinner, and S.M. Angel, *Comparative study of some fiber-optic remote Raman probe designs .2. Tests of single-fiber, lensed, and flat- and bevel-tip multi-fiber probes*. Applied Spectroscopy, 1996. **50**(7): p. 849-860.
33. Stokes, D.L. and T. Vo-Dinh, *Development of an integrated single-fiber SERS sensor*. Sensors and Actuators B-Chemical, 2000. **69**(1-2): p. 28-36.
34. Zhang, Y., et al., *Surface-enhanced Raman scattering sensor based on D-shaped fiber*. Applied Physics Letters, 2005. **87**(12).
35. Beam, B.M., et al., *Planar fiber-optic chips for broadband spectroscopic interrogation of thin films*. Applied Spectroscopy, 2007. **61**(6): p. 585-592.
36. Beam, B.M., N.R. Armstrong, and S.B. Mendes, *An Electroactive Fiber Optic Chip for Spectroelectrochemical Characterization of Ultra-Thin Redox Active Films*. Analyst, 2009. **134**: p. 454-459.
37. Schedin, F., et al., *Detection of individual gas molecules adsorbed on graphene*. Nature Materials, 2007. **6**(9): p. 652-655.
38. Fowler, J.D., et al., *Practical Chemical Sensors from Chemically Derived Graphene*. ACS Nano, 2009. **3**(2): p. 301-306.
39. Das, A., et al., *Monitoring dopants by Raman scattering in an electrochemically top-gated graphene transistor*. Nature Nanotechnology, 2008. **3**(4): p. 210-215.
40. Zhang, Z.Y., et al., *Self-referencing in optical-fiber surface plasmon resonance sensors*. IEEE Photonics Technology Letters, 2007. **19**(21-24): p. 1958-1960.
41. Alonso, R., et al., *NEW IN-LINE OPTICAL-FIBER SENSOR-BASED ON SURFACE-PLASMON EXCITATION*. Sensors and Actuators a-Physical, 1993. **37-8**: p. 187-192.
42. Tseng, S.M. and C.L. Chen, *SIDE-POLISHED FIBERS*. Applied Optics, 1992. **31**(18): p. 3438-3447.
43. Ding, L., D.N. Yuan, and J. Liu, *Growth of high-density parallel arrays of long single-walled carbon nanotubes on quartz substrates*. Journal of the American Chemical Society, 2008. **130**(16): p. 5428-+.
44. Reina, A., et al., *Layer Area, Few-Layer Graphene Films on Arbitrary Substrates by Chemical Vapor Deposition*. Nano Letters, 2009. **9**(8): p. 3087-3087.
45. Ruddy, V., B.D. Maccraith, and J.A. Murphy, *EVANESCENT WAVE ABSORPTION-SPECTROSCOPY USING MULTIMODE FIBERS*. Journal of Applied Physics, 1990. **67**(10): p. 6070-6074.
46. Baia, M., et al., *Probing the enhancement mechanisms of SERS with p-aminothiophenol molecules adsorbed on self-assembled gold colloidal nanoparticles*. Chemical Physics Letters, 2006. **422**(1-3): p. 127-132.
47. Shim, M.G., et al., *Study of fiber-optic probes for in vivo medical Raman spectroscopy*. Applied Spectroscopy, 1999. **53**(6): p. 619-627.
48. Maher, R.C., et al., *Temperature-Dependent Anti-Stokes/Stokes Ratios under Surface-Enhanced Raman Scattering Conditions*. The Journal of Physical Chemistry B, 2006. **110**(13): p. 6797-6803.
49. Maher, R.C., et al., *A study of local heating of molecules under Surface Enhanced Raman Scattering (SERS) conditions using the anti-Stokes/Stokes ratio*. Faraday Discussions, 2006. **132**: p. 77-83.

50. Lu, Y., G.L. Liu, and L.P. Lee, *High-density silver nanoparticle film with temperature-controllable interparticle spacing for a tunable surface enhanced Raman scattering substrate*. *Nano Letters*, 2005. **5**(1): p. 5-9.
51. Xie, L.M., et al., *Graphene as a Substrate To Suppress Fluorescence in Resonance Raman Spectroscopy*. *Journal of the American Chemical Society*, 2009. **131**(29): p. 9890-+.

CURRICULUM VITAE

Jennifer Burnett

7507 McIntosh Way, Louisville, KY 40228
(502)727-1063 • jennifer.burnett@louisville.edu

Education

University of Louisville
M.S., Physics
Current GPA: 3.9
Projected graduation: August 2010

University of Kentucky
B.S., Physics, Honors Program,
Minor: Mathematics
Graduated May 2005; GPA: 3.3

Professional Experience

Johns Hopkins Applied Physics Laboratory (May 2009 – August 2009)
Intern, Terahertz Spectroscopy Lab

Elemental Analysis (December 2006 – August 2008)
PIXE Lab Director, (Proton Induced X-ray Emission)

Elemental Analysis (April 2006 – December 2006)
Lab Technician

Awards

The Manuel Schwartz Award for Outstanding Graduate Performance in Physics, 2010

Publications

M.R. Leahy-Hoppa, J. Miragliotta, R. Osiander, J. Burnett, Y. Dikmelik, C. McEnnis, J.B. Spicer, Ultrafast Laser-Based Spectroscopy and Sensing: Applications in LIBS, CARS, and THz Spectroscopy, *Sensors* **2010**, *10*(5), 4342-4372

Presentations

Planar Fiber-Optic Chip for Fully Guided Raman Interrogation of Molecular Adsorbates, 2010 Kentucky Innovation and Entrepreneurship Conference Poster Session

Computer Expertise

Operating systems: Windows, DOS, and Linux based systems.
Programming languages: Fortran90